Arab American University

Faculty of Graduate Studies

Development of a Material Model for Stress Calculations in Lithium-ion Batteries

By

Dima Fuad Abubaker

Supervisor

Dr. Muayad Abu Saa

Co-Supervisor

Dr. Robert Mücke

This thesis was submitted in partial fulfillment of the requirements for the Master's degree in Applied Mathematics.

December, 2021

Development of a Material Model for Stress Calculations in Lithium-Ion Batteries

By

Dima Fuad Abubaker

This thesis was defended successfully on December 14, 2021 and approved by:

Committee Members	Signature
1. Supervisor: Dr. Muayad M. A. Abu Saa	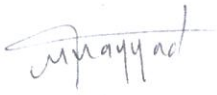
2. Co-Supervisor: Dr. Robert Mücke	
3. Internal Examiner: Dr. Iyad Suwan	
4. External Examiner: Dr. Adnan Daraghmeh	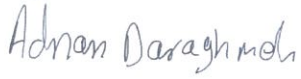

Declaration

I declare that this thesis entitled "Development of a Material Model for Stress Calculations in Lithium-ion Batteries" is my own work and has been composed solely by myself and does not contain any work form other researchers and has not been submitted for any other degree.

Date: August 21, 2022

Name	Signature
Dima Fuad Abubaker	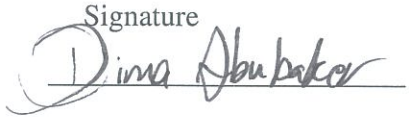

Acknowledgment

I would like to express my appreciation and deepest gratitude to my supervisors Dr. Muayad Abu-Saa and Dr. Robert Mücke for their valuable support and guidance, and for their valuable discussions.

A special thanks also goes to Dr. Ashraf Hadoush for introducing me to the new topic, to my colleagues in the modeling team Najma, Fadi and Ashutosh, who helped me throughout my research and were always patient for my endless questions.

Thanks to Prof. Dr. Oliver Guillon, director of the Institute of Energy and Climate Research IEK-1 in Forschungszentrum Jülich, for his valuable comments in the interviews and presentations.

Thanks for Forschungszentrum Jülich and their staff for hosting the research for my master thesis, to the PGSB for funding my stay in Germany while doing my research.

Finally, I would like to thank my family, my mother, sister and my brother and his wife for their endless support.

Abstract

All Solid state lithium-ion batteries are a promising source of energy for the newly developed small devices due to their safety and high capacity. However, these kinds of batteries still experience a volume change in their composite cathode structure leading to magnificent deformations and high stresses that will cause a fatigue in their material structure. One of the solutions to overcome this problem is to add elastomers in specific amounts to the composite cathode material with small to no effect on the cathode conductivity. In order to determine the best amount of elastomers, computer-based simulation is used to study the behaviour of the composite cathode after adding the elastomers. Previous stress-strain results obtained from modeling the hyperelastic compressible material behaviour of elastomers using small strain theory are promising but inaccurate. In order to obtain more accurate hyperelastic material behaviour, we use the large strain theory to model the elastomers' behaviour. We derive the equations required to represent the hyperelastic behaviour of the material properties using large strain theory. We implement the derived equations in Fortran and use this implementation to integrate the new hyperelastic behaviour into ANSYS and GeoDict. Our initial results show more accurate stress-strain values which means that the new hyperelastic behaviour model has a potential to be improved and used in future works.

Contents

List of Tables

List of Figures

Chapter 1

Introduction

Traditional lithium-ion batteries that contain liquid electrolyte have some disadvantages like suffering from flammability, electro-chemical stability and limited temperature range. To overcome these problems, all solid state lithium-ion batteries are now considered in modern studies. Extensive research is undertaken for this kind of batteries as an alternative power source. An all-solid-state battery is similar to a liquid electrolyte battery but it employs a solid electrolyte. As usual, it consists of three major parts: the cathode, the anode and the separator (the solid electrolyte) [1].

Lithium-ion batteries still suffer from mechanical fatigue caused by stress generation due the lithiation and delithiation in the charging and discharging processes. These lithiation and delithiation processes cause volume changes by expanding or shrinking the lattice of the composite cathode active material [9]. As a result, the researchers are trying to improve the efficiency for this battery type by improving the microstructure of their material and understand the electrochemical and electromechanical behaviour that occurs during the charging and discharging processes.

Simulating and modeling the structure of the composite cathodes with adding binders will give improved accurate stress results, and calculating the electrochemical induced stresses will give a better understanding of the deformations occurring during the charging and discharging processes.

In this work, we simulate the deformations that occur during the delithiation process in the composite cathode material. To achieve this, we use three different material bahaviours in the finite element ANSYS software: the simple linear anisotropic for the lithium cobalt oxide (LCO), the hyperelastic nonlinear for the polyethylene oxides (PEO), and the isotropic elastic for the lanthanum lithium zirconium oxide (LLZ).

ANSYS has the ability to model complex material responses such as the nonlinear and anisotropic elastic material behaviours. These kinds of models for complex material behaviour will reduce the efforts and the time consumed by the real-world experiments that try to calculate the generated stresses in the all-solid state lithium-ion batteries.

Although the ANSYS software is capable of modeling the behaviour of LCO and LLZ, it does not include all of the complex material behaviour models to cover PEO. Therefore, the hyperelastic nonlinear material for PEO needs to be introduced to ANSYS in order to be able to correctly analyze the model. To achieve this, we utilize the Blatz-Ko model of large strain theory in Our calculations to represent the PEO response.

We derive both of the Cauchy stress and the fourth order elasticity tensor (the stiffness matrix) required for analyzing the compressible, hyperelastic and nonlinear material behaviour for the PEO material. We implement these two equations in Fortran to include them then into ANSYS in order to build the whole model for the realistic microstructure of the composite cathode.

Our theoretical work builds up on a previous work of A. Hadoush [10] as follows: The previous work considers applying specific values for the Passion's ratio and the interpolation parameter ($\nu = 0.25$, and $f = 0.0$) of the strain energy function of Blatz-Ko model, whereas in our work we derive the Blatz-Ko function in the general form in order to represent the hyperelastic behaviour for different types of material. The previous work consider finding the stress-strain curves for different values of B, in our work we find the stress-strain curves with employing different values of f parameters.

The procedure of our work is as follows: First, we build a single model for analyzing the PEO model under structural loads. Then, we add LCO to the first model to represent

and include the chemical loads and strains. Finally, we build the real microstructure for the composite cathode by adding LLZ material (the geometry for this model was built using GeoDect and we used CGAL 5.2 for meshing).

This thesis is organized as follows: the first chapter gives the necessary background information and literature review. The second chapter explains the theory used in our model with the derivation of the strain energy function. Chapter four gives the procedure of building the models using ANSYS. Finally, the results are presented in chapter five and the thesis is concluded in chapter six.

Chapter 2

Background and Literature Review

2.1 Introduction to All-Solid-State Lithium-Ion Batteries (ASSB)

The first commercial use of lithium-ion batteries was by Sony in 1991, they became one of the most effective storage energy devices. The rapid development in industries especially small devices industries and the need for clean energy carriers render the unconventional all-solid-state lithium-ion batteries recently the best choice to be used as electrochemical energy storage devices to operate electric vehicles and mobile and electronic devices [11]. These kinds of batteries are the optimal alternative over the traditional lithium batteries because of their high electromechanical stability, energy density and low self-discharge rate. In addition to that, they can operate over a wider temperature rate (25-50°C) [4].

The main structure of the ASSB is similar to liquid state lithium batteries but with employing inorganic solid state electrolyte as separator. As seen in Figure 2.1, an ASSB cell has two electrodes (the anode and the cathode) and the solid state electrolyte with attaching current collector (copper to the anode and aluminum to the cathode to improve the electrical conductivity of the battery.

Cathodes supply lithium ions during the charging process (they are delithiated), and during the discharging process these ions will be stored in it (they are lithiated). For a

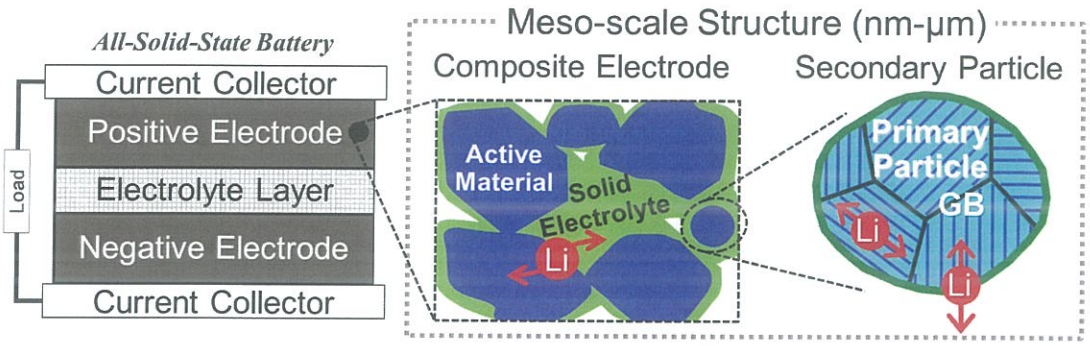

Figure 2.1: Schematic illustration of a positive electrode in an all-solid-state LIB [2]

stable lithiation and delithiation processes, it is critical that the structure of the cathode is mechanically stable provides a good ionic conductivity. During the charging process, lithiation takes place at the anode. The anode layered structure intercalates the lithium ions during the lithiation/delithiation process. The diffusion of the ions within the electrolyte is the critical performance limiting step in the solid state batteries. The main requirements for the solid state electrolytes are to exhibit ionic conductivity and very low electronic conductivity and to exhibit a high degree of chemical stability. It has been found that crystalline materials such as lithium halides, lithium nitrides, oxy-salts, and sulfides are suitable as solid electrolytes [12]. Oxides based ceramic solid electrolytes such as $Li_7La_3Zr_2O_{12}$ are widely used for their conductivity and high conductivity and chemical stability compared with the other type of electrolyte materials. The drawback for this kind of material is the need for high temperature during the sintering process. Several studies have been undertaken to calculate the performance for all-solid-state batteries in order to find an optimum microstructure for electrode materials. For this purpose, many techniques were used to calculate and and simulate the inner face of the solid state batteries electrodes and electrolyte. For example the nontrivial change to the internal LCO microstructure was studied, using a newly technique employing numerical calculations developed to estimate the generated stresses in the polycrystalline secondary particle of $LiCoO_2$ during the first charging process [2].

Another kind of research took in consideration the effect of anisotropic properties of the layered oxides in the cathode design, calculated the stresses in the composite cathodes

for all-solid-state batteries and compared them with isotropic case while focusing on the texture of the crystallographic alignment of LCO grains during manufacturing process. Another method for calculating the mechanical stress and electrochemical performance of the cathode microstructure, is including phase transition and Li intercalation using synchrotron X-ray nickel-manganese-cobalt (NMC) half cell with finite element method was proposed in [13]. The authors of [11] developed a framework of finite element method for simulating the anisotropy swelling and stress generation in Li ion batteries percolating network, they concluded that the development of stresses in the microstructure depends on the geometry and the particle size and the surface roughness.

2.2 Cathodes for Lithium-Ion Batteries

All-solid-state batteries contain electronic and ionic conductive composite cathodes unlike the traditional liquid state batteries. The common material for Lithium cathodes the transition metal oxides such as lithium cobalt oxides ($LiCoO_2$) and lithium manganese oxide ($Li_2Mn_2O_4$) due to their high theoretical specific capacity, safety and their high energy density and easy preparation.

$Li_2Mn_2O_4$ has a theoretical capacity of 110 mAh/g [14], on the other hand $LiCoO_2$ has a theoretical capacity of 270 mAh/g when being fully delithiatited. Another used cathode material is lithium-based phosphate ($LiFePO_4$), this material is less hazardous and low cost compared to other lithium oxide materials but has a low energy density.

Table 2.1: Electrochemical characteristics of the cathode materials [1]

	$LiCoO_2$	$LiNi_{0.80}Mn_{0.10}Co_{0.10}O_2$	$LiNi_{0.80}Co_{0.15}Al_{0.05}O_2$	$Li_2MnO_3LiNi_xMn_yCo_zO_2$	$LiFePO_4$	$LiNi_{1/3}Mn_{1/3}Co_{1/3}O_2$	$LiMn_2O_4$
Structure	Layered	Layered	Layered	Layered	Olivine	Layered	Spinel
Theoretical Capacity [mA h g^{-1}]	274	275	279	–	170	275	148
Available Capacity [mA h g^{-1}]	190@4.45V	210	200@4.3V	250@4.6V	160	160@4.3V	110
	215@4.55V		210@4.4V			185@4.5V	
Electrode Density [g cm^{-3}]	3.9	3.2	3.4	2.7	2.3	3.4	3.2
Galvanometric Energy Density [Wh kg^{-1}]	740@4.45V	800@4.4V	760@4.3V	900@4.6V	540	610@4.3V	410
	840@4.55V		800@4.4V			730@4.5V	
Volumetric Energy Density [Wh L^{-1}]	2900@4.45V	2600@4.4V	2600@4.3V	2430@4.6V	1240	2080@4.3V	1300
	3300@4.55V		2700@4.4V			2480@4.5V	
Operating Voltage [V]	3.9	3.8	3.8	3.6	3.4	3.8	4.0
Application	Mobile IT devices Power tools	Power tools Evs Energy storage Systems (ESSs)	Power tools Evs ESSs		Evs ESSs (low end)	Power tools Evs ESSs	Power tools Evs ESSs

2.3 LCO cathodes

2.3.1 Crystallographic of LCO

The high temperature synthesized $LiCoO_2$ (HT-$LiCoO_2$) has excellent electrochemical and structural stability. Thanks to their preserving the order of layered cation for LCO during the lithiation and delithiation process [5]. $LiCoO_2$ has hexagonal symmetry structure with cell parameters a=2.13 $A°$ and c=14.9 $A°$. Li and Co ions layered alternately as octahedral sites between the closed-pack cubic oxygen planes as shown in Figure 2.2 [5].

The importance of studying the LCO structure lies in providing the best pathway for Li ions during migration and intercalations of the ions in and out of the lattice of the crystal cathode structure during the charging and discharging process. The structure of the layered LCO cathode will experience a lot of change during the lithiation and delithiation processes. The method of single crystal X-ray diffraction has been done with studying the electrochemical and chemical properties for LCO material in order to understand the structural changes of LCO [15].

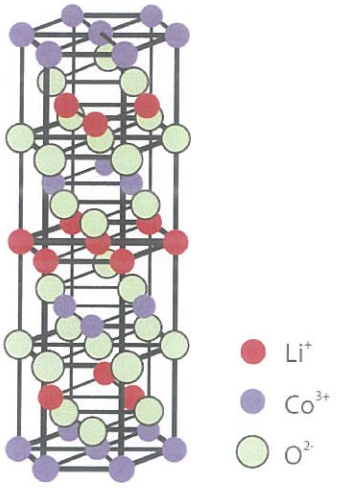

Figure 2.2: Layered LCO structure [3]

2.3.2 Deformations in Cathodes during Delithiation Process

During the discharging process the ions will leave the anode and the migration process of the ions takes place through the electrolyte again to reach the cathode to fill the empty octahedral sites in the layered cathode [3]. During the charging process (delithiation of the cathodes) lithium ions leave cathode structure and transfer to the anode through the solid electrolyte. In commercial batteries, the limit of typical reversible delithiation of $LiCoO_2$ is $x \approx 50\%$ [1]. During this operation the lithium concentration will decrease from 100% to 50%. The $LiCoO_2$ will slightly decrease in the a and d directions by 0.23%, due to the oxidation of Co. However, $LiCoO_2$ it will expand in c direction by 2.39% [16], due the increase in the electrostatic repulsion between two neighbouring oxygen layers.

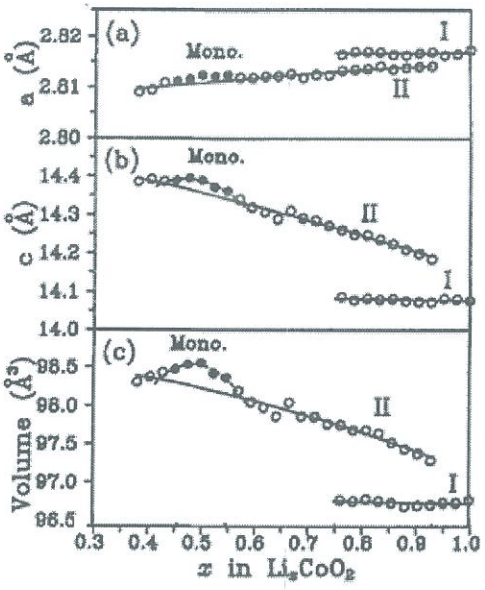

Figure 2.3: Variation of lattice parameters and unit cell volume, and crystalline phases present as functions of degree of lithiation of Li_xCoO_2 [4]

As shown in Figure 2.3, Li_xCoO_2 cathodes face different structural changes when the lithium is removed from their layered structure. For lithium concentration of $x = 1.0$, the cathode faces initial single phase I till x=0.9, the lattice parameter in c-axis increases monotonically and decreases for a-axis. From x=0.9 till x=0.78 two different phases will exist: the single initial phase I and phase II. In phase II, the lattice parameters are different from the initial phase I. From x=0.78 till x=0.51 the cathode faces a progressive increase in c-axis and a decreases in a-axis, the unit volume decrease by 3%. Below x=0.51 and till x=0.54 the hexagonal phase converts to monoclinic phase, and it remains as a single phase from x=0.45 till x=0.22 [4]

This change in the crystal structure will lead to crack formation in the LCO grains as shown in Figure 2.4, the cracks formed by lattice strains. The result of these repeating phase transformations will lead to damage of the electrical performance of the battery. Also the cathode material will face mechanical strain and stress which also leads to weakening the battery performance [3].

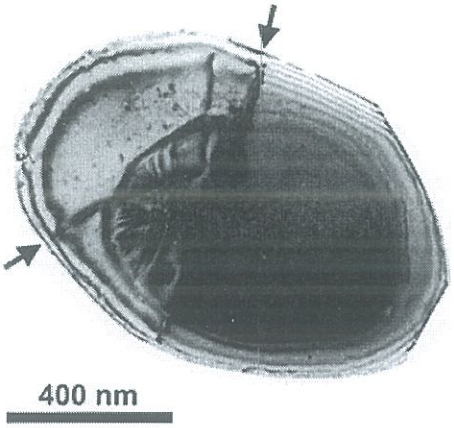

Figure 2.4: Severely damaged $LiCoO_2$ particles from a cycled cathode showing microfracture from internal strain and extended defects [5].

As a result a significant anisotropic volume expansion occurs in the storage material and since there is no free space between the solid phases there will be a development of high stresses and this will lead to mechanical fatigue during the cycling process.

In order to model these mechanism of stress generation and the effect of volume changing in the cathode microstructure, a 3D reconstruction of $LiCoO_2$ cathodes was carried out by scanning electron microscopy imaging [17].

2.3.3 Stiffness of LCO

To study the mechanical properties and the stiffness matrix components (elasticity tensors) for fully and partially lithiated LCO many techniques have been used experimentally and theoretically. Based on the three LCO structures shown in Figure 2.5 LCO elastic constant were calculated using the projector augmented wave method (PAW) [2], with the General Utility Lattice Program (GULP) [18] based on lattice model calculations to give the stiffness tensors as a result using theoretical stiffness tensors and estimated values for the thermal expansion coefficient of $LiCoO_2$ [19].

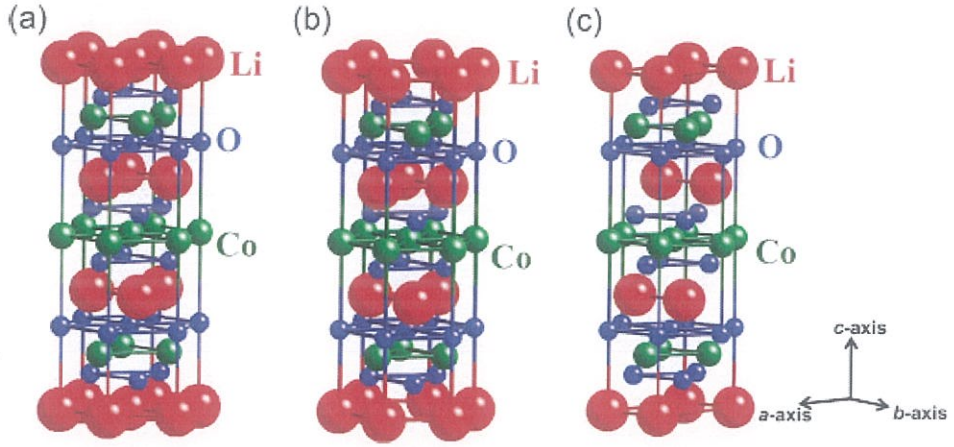

Figure 2.5: Crystal structures of (a) $LiCoO_2$, (b) $Li_{0.75}CoO_2$, and (c) $Li_{0.5}CoO_2$ [2].

Table 2.2 shows a comparison between three cases of fully and partially lithiated $LiCoO_2$ elastic constants (x=1, 0.75, 0.5) in Voigt notation. For the fully lithiated LCO, two studies applying different methods, PAW [2] and lattice mechanics method [19], were reported. The experimental results for the bulk modulus (146.66 GPa) almost agree with calculations results (149 GPa) using the Hills approximation [2].

Table 2.2: Components of the elastic stiffness tensor of LCO at different degrees of lithiation, C_{mn} [2].

Component	C_{mn} (GPa)			
	$LiCoO_2$		$Li_{0.75}CoO_2$	$Li_{0.5}CoO_2$
	Present study	Lattice mechanics [23]	Present study	Present study
11	339.79	596.4	325.75	303.86
12	101.6	199.4	95.59	100.71
13	65.78	133.5	50.14	32.58
14	−6.39	−8.28	5.70	0
15	0	0	0	7.31
22	C_{11}	C_{11}	C_{11}	318.93
23	C_{13}	C_{13}	C_{13}	28.66
25	0	0	0	−3.93
33	214.67	375.2	158.0	98.93
35	0	0	0	7.03
44	51.47	124.1	32.77	18.02
46	0	0	0	−2.46
55	C_{44}	C_{44}	C_{44}	15.73
66	$(C_{11} - C_{12})/2$	$(C_{11} - C_{12})/2$	$(C_{11} - C_{12})/2$	101.94

The anisotropic shape for the $Li_{0.5}CoO_2$ stiffness matrix was calculated in another

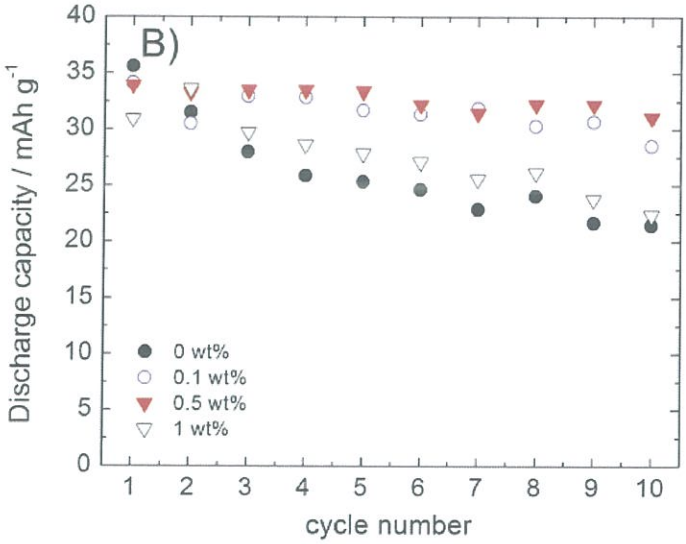

Figure 2.6: Cycle performance of glass/cathode composite using NCM particles coated with the Li_6PS_5Cl solid electrolyte and different content of binder [6].

In a promising study [6], small amounts of binder (5 wt%) were added to composite cathodes with high content of active material (89 wt%). It was shown that this improved the cycle life when using 0.1-0.5 wt% for all solid state batteries as shown in Figure 2.6. Too much binders added lead to encapsulation of the active material.

In a previous study on the effects of adding specific amount of elastomers (PEO) to the composite cathode material R. Muecke found that elastomers allow large decreases in stresses and they undergo large strains (20% and more). The first try for stress-strain calculations (using the small strain theory) shows a general improving effect in decreasing the stress values as shown in Figure 2.7. Figure 2.8 shows the binders in the composite cathode undergo large deformations/strains (20% and more).

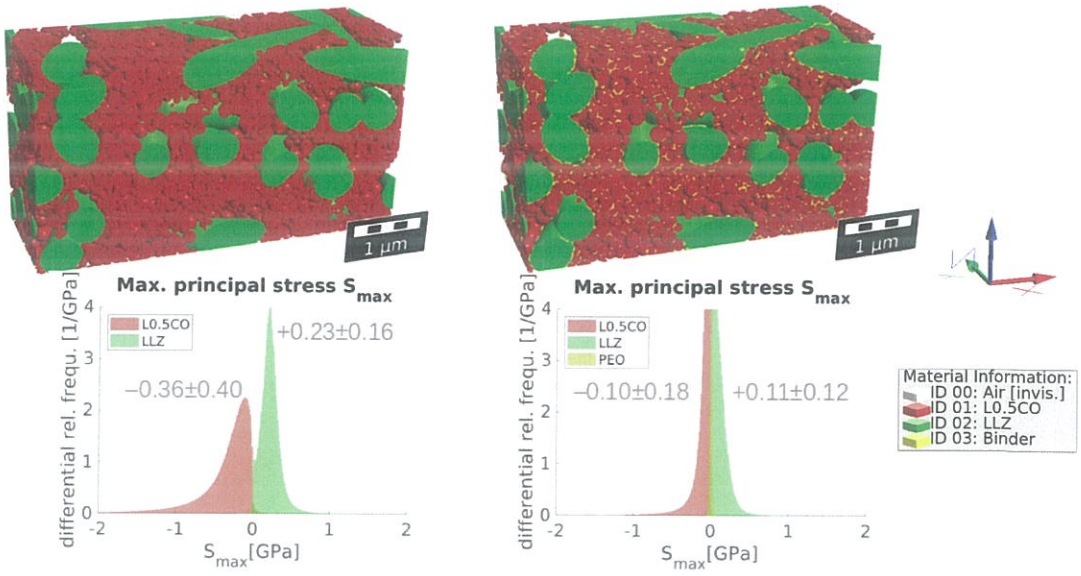

Figure 2.7: Stress results with and without adding elastomers on the composite cathode material.

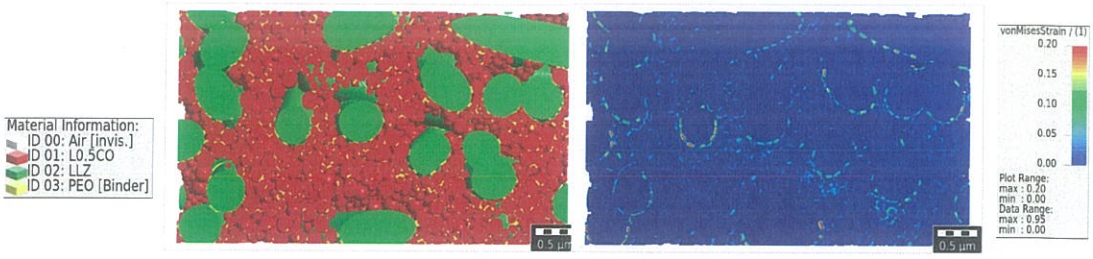

Figure 2.8: Strain results with adding elastomers in composite cathode material.

Because of the nonlinear hyperelastic material behaviour of elastomers, the small strain theory is not effective to find an accurate stress-strain relationship. Because of that, this study will focus on studying the material behaviour of elastomers and used the appropriate method for stress strain calculations.

2.5 Mathematical Representation for Hyperplastic Compressible Material Behaviour

Hyperelastic material (nonlinear material) or Green material are a commonly used terms and models to describe the material behaviour of elastomers, rubbers and foamed material. They have in common a large strain response during applied loads [25]. Hyperelasticity is a special case of a Green material, the strain relationships can be derived from their constitutive or strain energy density function depending on the deformation gradient or the strain tensor.

The physical idea behind the isotropy is that when a load is applied in stress strain experiments the response of the material will be the same in all directions. The definition of compressibility means that the material can undergo changes of volume. Material with the Poisson's ratio less than 0.5 are compressible such as rubber and gases. On the other hand the material with Poisson's ratio of 0.5 are perfectly incompressibe. These materials keep the volume constant under deformation.

Studying the performance of hyperelastic materials under different states of deformation by employing traditional phenomenological and mechanical models [26] is covered in the excellent survey by Hoassain and Steinmann [26].

In a study that considers finding the stress-strain curves using the material properties parameters [27], the data were taken from applying two kinds of deformation: simple tension and equibiaxial extension. These two deformations were used to model rubberlike material using new and unique invariants such as Seth strain tensor (E^n). When $n \neq 0$, the expression of E^n is defined as $E^n = \frac{1}{2n}(C^n - I)$ where C is the right Cauchy-Green tensor and I is the identity matrix [25].

Some commonly used compressible hyperelastic models such as Moony-Relivin and Ogden model employ the constitutive equation's or the strain energy function to specify the stress components in terms of strain invariants or principal stretches. Some mathematicians and scientists improved these models by adding more parameters to use in the

strain energy function in order to derive analytical and numerical solutions [28]. Other scientist added a novel new micromechanical hyperelastic models by applying a distribution function [29]. We choose the Blatz-Ko model as the strain energy function because it represents the compressible hyperelastic material as a one-part function with the strain invariants. This function is easy to derive and easily adaptable to even more complex material behaviours.

2.5.1 Large Strain theory

In continuum mechanics, the small strain theory, or the Cauchy elastic behaviour, means that the strains are small (less than 5%) and the deformation of the body is almost negligible. For this case, the stress-strain relationship is linear and the strain energy function in the reference configuration (Normalized condition) is almost equal to that of the current configuration. This is not the case for the large strain theory: the deformation of the body is not negligible anymore as strains are large (more than 5%) and the reference and the current configuration are not equal any more.

The main characteristic for large strain theory for deformable bodies is the existence of the strain energy function. The strain or stored energy function (Helmholtz free-energy function Ψ) is a scalar valued function of one tensor variable such as the strain tensor, or set of independent strain invariants of C and b which are the right and left Cauchy Green tensors [30]. There are new concepts for this theory: the reference configuration means that the position vector is not deformed, and when deformation occurs the position will be in the current configuration as shown in Figure 2.9. The stress is different in the current configuration because it is a function of strain tensor or a function of deformation gradient, and the deformation gradient in current configuration is different from that of reference configuration.

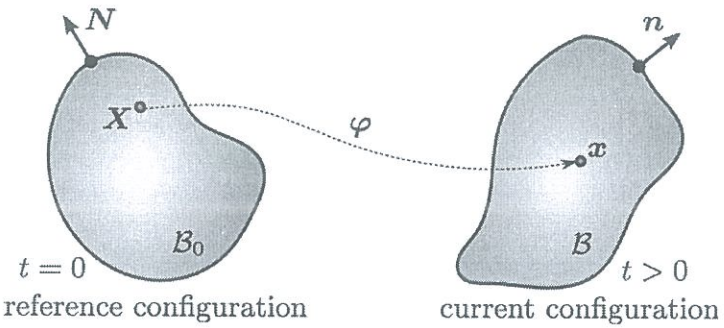

Figure 2.9: Schematic representation of the relationship between reference and current configuration [7].

2.5.2 The Blatz-Ko Model

Many finite element analysis models exist to represent and model the hyperelastic material behaviour such as New Hooken, Varga model, Mooney-Rivajin and Arruda and Boyce model. All of these models represent the incompressible behaviour that undergoes very small volume changes with the assumption that the volume ratio as $J=\frac{V}{V_0} \approx 1$. The previous models can also be represented as compressible material behaviour as strain energy function that consists of two parts. The first part describes the purely isochoric elastic response, whereas the second part describes the purely volumetric elastic response. The strain energy function depends on the strain tensor C and $C = J^{\frac{2}{3}}\overline{C}$. $J^{\frac{2}{3}}$ is the volume ratio and this part is related to the volume changing deformation. The other part $\overline{C}$ is the modified right Cauchy-Green tensor and is associated with volume preserving deformation.

Blatz and Ko model (1962) is a mathematical representation for the mechanical behaviour for a highly elastic or perfectly elastic rubber-like material at a fixed temperature, employing a unique strain energy form [31].

$$\Psi(I_1,I_2,I_3) = \mathfrak{f}\frac{\mu}{2}[(I_1-3)+\frac{1}{B}(I_3^{-B}-1)]+(1-\mathfrak{f})\frac{\mu}{2}[(I_2I_3^{-1}-3)+\frac{1}{B}(I_3^{B}-1)] \quad (2.1)$$

where $\Psi(I_1, I_2, I_3)$ is the strain energy function

$\mathfrak{f} \in [0,1]$ is an interpolation parameter

μ is the shear modulus

C is the right Cauchy-Green tensor, $C = F^T F$

F is the deformation gradient

B $= \dfrac{\nu}{1-2\nu}$ where ν is Poisson's ratio

I_1 $= tr(C)$

I_2 $= \dfrac{1}{2}[(tr(C))^2 - tr(C^2)]$.

I_3 $= \det C$.

It is the most suitable model for describing the nonlinear hyperelastic compressible material behaviour of PEO as a coupled function of volumetric and isochoric parts. This makes it easy to derive the elasticity tensor from the strain energy function which combines the theoretical and the previous experimental data [32].

Chapter 3

Modelling of Hyperelastic Nonlinear Material Behaviour Using Large Strain Theory

3.1 Derivation of Quantities from the Blatz-Ko Model

As mentioned in chapter two, the description of the hyperelastic material behaviour of PEO needs to follow the large strain theory. In order to consider the compressible behaviour of PEO, the Blatz-Ko model is used. The Cauchy stress and the forth order elasticity tensor have to be derived from the stain energy function of the Blatz-Ko model given in (2.1).

In order to derive the Cauchy stress and the fourth order elasticity tensor from the strain energy function related of the Blatz-Ko model, we give the first partial derivatives with respect to the invariants as follows:

$$\frac{\partial \Psi(I_1, I_2, I_3)}{\partial I_1} = f\frac{\mu}{2}, \tag{3.1}$$

$$\frac{\partial \Psi(I_1, I_2, I_3)}{\partial I_2} = (1-f)\frac{\mu}{2}I_3^{-1}, \tag{3.2}$$

$$\frac{\partial \Psi(I_1,I_2,I_3)}{\partial I_3} = -f\frac{\mu}{2}I_3^{-B-1} - (1-f)\frac{\mu}{2}I_2 I_3^{-2} + (1-f)\frac{\mu}{2}I_3^{B-1}, \tag{3.3}$$

and with respect to the second partial derivatives as follows:

$$\frac{\partial^2 \Psi(I_1,I_2,I_3)}{\partial I_1 \partial I_1} = 0, \tag{3.4}$$

$$\frac{\partial^2 \Psi(I_1,I_2,I_3)}{\partial I_1 \partial I_2} = 0, \tag{3.5}$$

$$\frac{\partial^2 \Psi(I_1,I_2,I_3)}{\partial I_1 \partial I_3} = 0, \tag{3.6}$$

$$\frac{\partial^2 \Psi(I_1,I_2,I_3)}{\partial I_2 \partial I_1} = 0, \tag{3.7}$$

$$\frac{\partial^2 \Psi(I_1,I_2,I_3)}{\partial I_2 \partial I_2} = 0, \tag{3.8}$$

$$\frac{\partial^2 \Psi(I_1,I_2,I_3)}{\partial I_2 \partial I_3} = -(1-f)\frac{\mu}{2}I_3^{-2}, \tag{3.9}$$

$$\frac{\partial^2 \Psi(I_1,I_2,I_3)}{\partial I_3 \partial I_1} = 0, \tag{3.10}$$

$$\frac{\partial^2 \Psi(I_1,I_2,I_3)}{\partial I_3 \partial I_2} = -(1-f)\frac{\mu}{2}I_3^{-2}, \tag{3.11}$$

$$\frac{\partial^2 \Psi(I_1,I_2,I_3)}{\partial I_3 \partial I_3} = -(-B-1)f\frac{\mu}{2}I_3^{-B-2} + (1-f)\mu I_2 I_3^{-3} + (1-f)(B-1)\frac{\mu}{2}I_3^{B-2}. \tag{3.12}$$

3.1.1 Calculation of Cauchy Stresses

In order to find the Cauchy stress (the stress in current configuration), we first find the stress in reference configuration (Second Piola-Kirchhoff stress) and transfer this stress by Piola transformation. The second Piola-Kirchhoff stress (**S**) is

$$\mathbf{S} = 2\frac{\partial \Psi(I_1,I_2,I_3)}{\partial C} = 2\left(\frac{\partial \Psi(I_1,I_2,I_3)}{\partial I_1}\frac{\partial I_1}{\partial C} + \frac{\partial \Psi(I_1,I_2,I_3)}{\partial I_2}\frac{\partial I_2}{\partial C} + \frac{\partial \Psi(I_1,I_2,I_3)}{\partial I_3}\frac{\partial I_3}{\partial C}\right). \tag{3.13}$$

where $\frac{\partial I_1}{\partial \mathbf{C}}$ =$\mathbf{I}$ the identity matrix

$\frac{\partial I_2}{\partial \mathbf{C}}$ =$I_1\mathbf{I}-\mathbf{C}$. where $\mathbf{C}$ is the right Cauchy-Green tensor

$\frac{\partial I_3}{\partial \mathbf{C}}$ =$I_3\mathbf{C}^{-1}$

hence,

$$\mathbf{S} = f\mu + (1-f)\mu I_3^{-1} I_1 - (1-f)\mu I_3^{-1}\mathbf{C} + f\mu I_3^{-B}\mathbf{C}^{-1} - (1-f)\mu I_2 I_3^{-1}\mathbf{C}^{-1} + (1-f)\mu I_3^{B}\mathbf{C}^{-1} \quad (3.14)$$

In order to find the stress in the current configuration (the Cauchy stress (σ)) from (3.14) we use the deformation gradient (F) and the volume ratio (J) in Piola transformation as

$$\begin{aligned}\sigma &= J^{-1}F\mathbf{S}F^T \\ &= J^{-1}[f\mu\mathbf{b} + (1-f)\mu I_3^{-1} I_1\mathbf{b} - (1-f)\mu I_3^{-1}\mathbf{b}^2 + f\mu I_3^{-B}\mathbf{I} - (1-f)\mu I_2 I_3^{-1}\mathbf{I} + (1-f)\mu I_3^{B}\mathbf{I}] \\ &= J^{-1}\mu[(1-f)(I_3^{B} - \mathbf{b}^{-1}) + f(\mathbf{b} - I_3^{-B}\mathbf{I})].\end{aligned} \quad (3.15)$$

where $J^{-1} = I_3^{-\frac{1}{2}}$

$\mathbf{b}^2 = I_1\mathbf{b} - I_2\mathbf{I} + I_3\mathbf{b}^{-1}(Cayley - Hamilton)$

as a result of this transformation, the stress after this operation is in terms of the left Cauchy-Green tensor ($\mathbf{b}$). Another way we can find the Cauchy stress by deriving the strain energy function directly with respect to the left Cauchy-Green tensor ($\mathbf{b}$) as

$$\begin{aligned}\sigma &= 2J^{-1}\mathbf{b}\frac{\partial \Psi(I_1, I_2, I_3)}{\partial \mathbf{b}} \\ &= 2J^{-1}[(I_2\frac{\partial \Psi(I_1, I_2, I_2)}{\partial I_2} + I_3\frac{\partial \Psi(I_1, I_2, I_3)}{\partial I_3})\mathbf{I} + \frac{\partial \Psi(I_1, I_2, I_3)}{\partial I_1}\mathbf{b} - I_3\frac{\partial \Psi(I_1, I_2, I_3)}{\partial I_2}\mathbf{b}^{-1}]\end{aligned} \quad (3.16)$$

In tensor notation:

$$\sigma_{ij} = J^{-1}\mu[(1-f)J^{2B}(\delta_{ij} - \mathbf{b}_{ij}^{-1}) + f(\mathbf{b}_{ij} - J^{-2B}\delta_{ij})] \tag{3.17}$$

3.1.2 Calculation of Elasticity Tensor

In order to find the elasticity tensor in the current configuration, we first find the elasticity tensor in reference configuration ($\mathbb{C}$). To do so, we take the second derivative of the stain energy function with respect to the right Cauchy-Green tensor (C):

$$\mathbb{C} = \frac{\partial^2\Psi(I_1,I_2,I_3)}{\partial E \partial E} = 4\frac{\partial^2\Psi(I_1,I_2,I_3)}{\partial C \partial C} = 2\frac{\partial \mathbf{S}(C)}{\partial C} \tag{3.18}$$

where E is the Green-Lagrange strain tensor, $E = \frac{1}{2}(C-I)$.

Then, we find the elasticity tensor of the current configuration (spatial elasticity tensor $\mathbb{D}$) by the Piola transformation of $\mathbb{C}$ as

$$\mathbb{D} = J^{-1}FFFF\mathbb{C} \tag{3.19}$$

Or, we can find the spatial elasticity tensor by deriving the the strain energy function twice with respect to $\mathbf{b}$ as

$$\begin{aligned}
\mathbb{D} &= 4J^{-1}\mathbf{b}\frac{\partial^2\Psi(I_1,I_2,I_3)}{\partial \mathbf{b}\partial \mathbf{b}}\mathbf{b} \\
&= 4J^{-1}\mathbf{b}[\frac{\partial(\frac{\mu}{2}[(1-f)(J^{2B}\mathbf{b}^{-1}) + fJ^{-2B}\mathbf{b}^{-1} - (1-f)\mathbf{b}^{-2}])}{\partial \mathbf{b}}]\mathbf{b} \\
&= 4J^{-1}\mathbf{b}[\mu[fJ^{-2B}(B(\mathbf{b}^{-1}\odot\mathbf{b}^{-1}) - \mathbf{b}^{-1}\otimes\mathbf{b}^{-1}) + 2(1-f)J^{2B}(B(\mathbf{b}^{-1}\odot\mathbf{b}^{-1}) + \mathbf{b}^{-1}\otimes\mathbf{b}^{-1}) \\
&+ (1-f)(\mathbf{b}^{-2}\odot\mathbf{b}^{-1} + \mathbf{b}^{-1}\odot\mathbf{b}^{-2})]]\mathbf{b} \\
&= 2J^{-1}\mu[fJ^{-2B}(B(\mathbb{I}\odot\mathbb{I}) - \mathbb{I}\otimes\mathbb{I}) + 2(1-f)J^{2B}(B(\mathbb{I}\odot\mathbb{I}) + \mathbb{I}\otimes\mathbb{I}) \\
&+ (1-f)(\mathbf{b}^{-1}\odot\mathbb{I} + \mathbb{I}\odot\mathbf{b}^{-1})].
\end{aligned} \tag{3.20}$$

In tensor notation:

$$\mathbb{D} = J^{-1}\mu[fJ^{-2B}(2B(\delta_{ij}\delta_{kl}) + (\delta_{ik}\delta_{il} + \delta_{il}\delta_{jk})) + (1-f)J^{2B}(2B(\delta_{ij}\delta_{kl}) - (\delta_{ik}\delta_{il} + \delta_{il}\delta_{jk})) + (1-f)((\mathbf{b}_{ik}^{-1}\delta_{jl} + \mathbf{b}_{il}^{-1}\delta_{jk}) + (\delta_{ik}\mathbf{b}_{jl}^{-1} + \delta_{il}\mathbf{b}_{jk}^{-1}))]. \quad (3.21)$$

The implementation of the derived equations (3.16) and (3.20) represent the hyperealstic compressible material behaviour for PEO.

3.2 Implementing the Hyperealstic Compressible Material Behaviour into ANSYS

In this section, we explain how we integrate the hyperelastic compressible material behaviour for PEO into ANSYS in order to find the nonlinear stress-strain relationship for these materials.

3.2.1 UserMat in ANSYS

The user-material routine, or the USERMAT, is an ANSYS user programmable feature allowing the users to model and implement their own material behaviour by introducing the appropriate equations to ANSYS using the user defined functions (UDF) feature of the software. This feature allows the user to define the material behaviour as functions written in the FORTRAN programming language.

USERMAT has a subroutine called `usermat3d` and the header of this subroutine contains input, input-output and output arguments that are the possible quantities and definitions to define the equations needed to identify the different mechanical quantities such as stresses and strains, elastic and plastic work, stiffness matrix which are variables and constants used in the common constitutive equations. For our models, the most important argument is the deformation gradient F at time t (called defGrad in `usermat3d`'s input

arguments). F is defined as

$$F_{ij} = \frac{\partial x_i}{\partial X_j},$$

where X is the position in the reference configuration and x is the position in the current configuration. For 3D spaces,

$$F = \begin{bmatrix} F_{11} & F_{12} & F_{13} \\ F_{21} & F_{22} & F_{23} \\ F_{31} & F_{32} & F_{33} \end{bmatrix}.$$

The other input parameters that need to be defined are the strain energy function's parameters and constants: the shear modulus, Poisson's ratio and the interpolation parameter f.

3.2.2 Implementing the Derived Equations in Fortran

We use USERMAT to introduce the hyperelastic material behaviour for PEO to ANSYS by implementing the derived equations form the strain energy function (the Cauchy stress and the Spatial elasticity tensor matrices). To do so, we need to define the built-in parameters and new parameters based on our model.

In order to accommodate the equations of Cauchy stress (3.16) and Spatial elasticity tensor (3.20) in the USERMAT, we define both of the determinant of F J and F^{-1} in order to define the Left Cauchy Green tensor ($\mathbf{b}$) as $\mathbf{b} = FF^T$. $\mathbf{b}$ has to be defined as double-precision floating-point vector. In order to do this we need to convert the second order tensor to one dimensional vector using the Voigt notation as:

$$\mathbf{b}_{ij} = \begin{bmatrix} \mathbf{b}_{11} & \mathbf{b}_{12} & \mathbf{b}_{13} \\ \mathbf{b}_{31} & \mathbf{b}_{22} & \mathbf{b}_{23} \\ \mathbf{b}_{31} & \mathbf{b}_{32} & \mathbf{b}_{33} \end{bmatrix} = \mathbf{b}_i = \begin{bmatrix} \mathbf{b}_1 & \mathbf{b}_4 & \mathbf{b}_6 \\ \mathbf{b}_4 & \mathbf{b}_2 & \mathbf{b}_5 \\ \mathbf{b}_6 & \mathbf{b}_5 & \mathbf{b}_3 \end{bmatrix} = \mathbf{b} = \begin{bmatrix} \mathbf{b}_1 \\ \mathbf{b}_2 \\ \mathbf{b}_3 \\ \mathbf{b}_4 \\ \mathbf{b}_5 \\ \mathbf{b}_6 \end{bmatrix}$$

Algorithm 1 Components of Cauchy stress

$N = \mu J^{-1}$
for $i = 1$ to 3 **do**
  $\sigma_i = N[(1-f)(J^{2B} - \mathbf{b}_i^{-1}) + f(\mathbf{b}_i - J^{-2B})]$
end for
for $i = 4$ to 6 **do**
  $\sigma_i = N[f\mathbf{b}_i - (1-f)\mathbf{b}_i^{-1}]$
end for

Also, we need to do the same operation to the fourth order tensor (stiffness matrix) in Voigt notation. Due to the symmetry of the spatial elasticity tensor or the elasticity tensor, we can write the stiffness matrix as:

$$\begin{bmatrix} \mathbb{D}_{1111} & \mathbb{D}_{1122} & \mathbb{D}_{1133} & \mathbb{D}_{1112} & \mathbb{D}_{1123} & \mathbb{D}_{1113} \\ \mathbb{D}_{1122} & \mathbb{D}_{2222} & \mathbb{D}_{2233} & \mathbb{D}_{2212} & \mathbb{D}_{2223} & \mathbb{D}_{2213} \\ \mathbb{D}_{1133} & \mathbb{D}_{2233} & \mathbb{D}_{3333} & \mathbb{D}_{3312} & \mathbb{D}_{3323} & \mathbb{D}_{3313} \\ \mathbb{D}_{1112} & \mathbb{D}_{2212} & \mathbb{D}_{3312} & \mathbb{D}_{1212} & \mathbb{D}_{1223} & \mathbb{D}_{1213} \\ \mathbb{D}_{1123} & \mathbb{D}_{2223} & \mathbb{D}_{3323} & \mathbb{D}_{1223} & \mathbb{D}_{2323} & \mathbb{D}_{2313} \\ \mathbb{D}_{1113} & \mathbb{D}_{2213} & \mathbb{D}_{3313} & \mathbb{D}_{1213} & \mathbb{D}_{2313} & \mathbb{D}_{1313} \end{bmatrix} = \begin{bmatrix} \mathbb{D}_{11} & \mathbb{D}_{12} & \mathbb{D}_{13} & \mathbb{D}_{14} & \mathbb{D}_{15} & \mathbb{D}_{16} \\ \mathbb{D}_{12} & \mathbb{D}_{22} & \mathbb{D}_{23} & \mathbb{D}_{24} & \mathbb{D}_{25} & \mathbb{D}_{26} \\ \mathbb{D}_{13} & \mathbb{D}_{23} & \mathbb{D}_{33} & \mathbb{D}_{34} & \mathbb{D}_{35} & \mathbb{D}_{36} \\ \mathbb{D}_{14} & \mathbb{D}_{24} & \mathbb{D}_{34} & \mathbb{D}_{44} & \mathbb{D}_{45} & \mathbb{D}_{46} \\ \mathbb{D}_{15} & \mathbb{D}_{25} & \mathbb{D}_{35} & \mathbb{D}_{45} & \mathbb{D}_{55} & \mathbb{D}_{56} \\ \mathbb{D}_{16} & \mathbb{D}_{26} & \mathbb{D}_{36} & \mathbb{D}_{46} & \mathbb{D}_{56} & \mathbb{D}_{66} \end{bmatrix}$$

After defining the left Cauchy-Green tensor and its inverse with every constant in the strain function, we write the components for both of the Cauchy stress and the Spatial elasticity tensor as respectively shown in Algorithms 1 and 2. The full USERMAT that includes our implementation of Algorithms 1 and 2 is given in Appendix A.3.

Algorithm 2 Components of Spatial elasticity tensor

$N = \mu J^{-1}$
for $i = 1$ to 3 **do**
  $\mathbb{D}_{i,i} = N[fJ^{-2B}(2B+2) + (1-f)J^{2B}(2B-2) + 4(1-f)\mathbf{b}_i^{-1}]$
end for
$\mathbb{D}_{44} = N[fJ^{-2B} + (1-f)J^{2B} + (1-f)\mathbf{b}_1^{-1} + \mathbf{b}_2^{-1}]$
$\mathbb{D}_{55} = N[fJ^{-2B} + (1-f)J^{2B} + (1-f)\mathbf{b}_2^{-1} + \mathbf{b}_3^{-1}]$
$\mathbb{D}_{66} = N[fJ^{-2B} + (1-f)J^{2B} + (1-f)\mathbf{b}_1^{-1} + \mathbf{b}_3^{-1}]$
$\mathbb{D}_{12} = \mathbb{D}_{13} = \mathbb{D}_{23} = N[fJ^{-2B}(2B) + (1-f)J^{2B}(2B)]$
$\mathbb{D}_{14} = 2N(1-f)\mathbf{b}_4^{-1}$
$\mathbb{D}_{15} = \mathbb{D}_{26} = \mathbb{D}_{34} = 0.0$
$\mathbb{D}_{16} = \mathbb{D}_{36} = 2N(1-f)\mathbf{b}_6^{-1}$
$\mathbb{D}_{24} = 2N(1-f)\mathbf{b}_4^{-1}$
$\mathbb{D}_{25} = \mathbb{D}_{35} = 2N(1-f)\mathbf{b}_5^{-1}$
$\mathbb{D}_{45} = N(1-f)\mathbf{b}_6^{-1}$
$\mathbb{D}_{46} = N(1-f)\mathbf{b}_5^{-1}$
$\mathbb{D}_{56} = N(1-f)\mathbf{b}_4^{-1}$
for $i = 1$ to ncomp-1 **do**
  for $j = i+1$ to ncomp **do**
    $\mathbb{D}_{ji} = \mathbb{D}_{ij}$
  end for
end for

Chapter 4

Implemented Models and Experiments

We built three different models to represent the three different material behaviours inside the composite cathode material targeted in our work (PEO, LCO, and LLZ). We used ANSYS 2020R2 mechanical software to simulate these models. ANSYS (analysis system) is one of the softwares used to solve linear and nonlinear problems and simulate the physical behaviour of complex engineering systems such as thermodynamics, solid and fluid mechanics with using the full Newton-Raphson scheme for a global solution to achieve better convergence rate [30]. We used SI units (m, kg, s, K) and the Cartesian coordinate system. The simulation had the following objectives:

- Representing the stress-strain relations by the definition of the large strain theory.
- Modeling a single material behaviour (the elastomers).
- Add the LCO with anisotropic behaviour to study stress-strain relation and the resulting deformations after applying the mechanical as well as the chemical strains during the lithiation process.

We followed the following steps to build each model:

1. Define the geometry of the structure by using the menu bar or APDL commands.
2. Selecting the appropriate element type for each model.

3. Selecting material properties parameters and constants such as Young's modulus, Poisson ratio for isotropic, components of stiffness matrix for anisotropic cases.

4. Specify the coefficients for the chemical-mechanically coupled structure models (lithiation expansion coefficient and saturation concentration).

5. Applying the structural boundary conditions such as the applying loads and structural constraints.

6. Select analysis type with solving choices (for hyperelastic case to activate true strains turn on the nonlinear solution option (NLGEOM,ON).

4.1 Model 1: Simple PEO Cube

Element Type

To simulate the hyperelastic nonlinear material behaviour for PEO, 3D SOLID 185 elements were used for the structural analysis; this element type has 8 nodes with 3 degrees of freedom for each node. In addition, this element type is suitable and capable of modeling the elastic, hyperelastic and creep behaviours in large deformations.

Creating Structural Geometries in ANSYS

The geometry for this model is simple, a cube with 1 mm dimension was built using 8 keypoints. Every keypoint has to be created by providing the location in Cartesian's coordinates (in the three directions X,Y,Z). After creating the keypoints, 6 areas have to be defined. The final step is creating the volume bounded by the 6 existing areas. After that meshing was performed to generate the nodes and elements within the volume. Figure 4.1 shows the simple PEO cube using the keypoints given in Table 4.1.

Table 4.1: Keypoint locations

keypoint number	1	2	3	4	5	6	7	8
keypiont location (X,Y,Z)	0,0,0	1,0,0	1,0,1	0,0,1	0,1,0	1,1,0	1,1,1	0,1,1

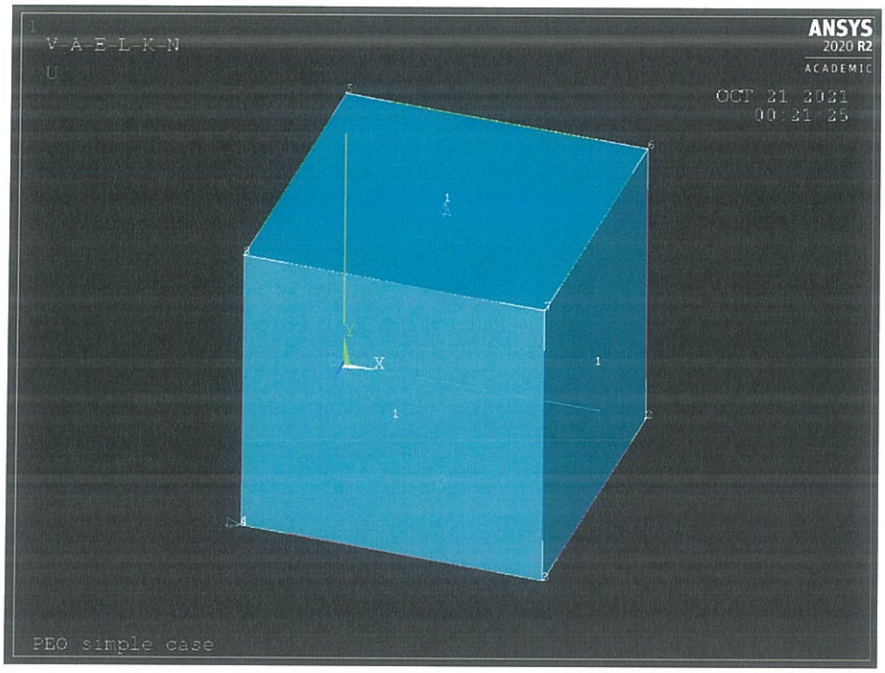

Figure 4.1: Structural Geometry for PEO Model

Material Parameters and Properties

The constants and parameters that are mentioned in the Blazt-Ko model (ν, μ and the interpolation parameter f) need to be define in the USERMAT file, and then their values were set in the main APDL code.

Loads and Boundary Conditions

In order to add the loads and the structural boundary conditions on both keypoints and areas, the degrees of freedoms are specified. The displacement degree of freedom for the bottom area in Y direction was set to zero (UY=0). In order to prevent the movement in the XZ plane, one point of the bottom area is completely fixed (UX=0,UY=0,UZ=0). The uniaxial tension and compression on the upper area are applied by a definite displacement.

For including large-deflection effects in this analysis we activate the command NL-

GEOM. When this is included the logarithmic strains included automatically.

4.2 Model 2: Sandwich LCO/PEO Sample

Element Types

This model represents the deformations on both LCO and PEO in the lithiation process. The structural-diffusion coupling analysis is used to represent the strains and deformations caused by volume changes in the lithiation process. Two different elements were used in ANSYS mechanical 2020 R2 in order to represent the PEO hyperelastic material behaviour and the LCO anisotropic elastic material behaviour: 3D SOLID 185 and SOLID 226, respectively.

SOLID 226 is appropriate to represent many coupled physical fields such as the structural-electrostatic, thermo-elastic, thermo-elastic-structural and as in our case the structural-diffusional analysis. SOLID 226 has 20 nodes with 6 degrees of freedom per node. It is capable of simulating large strains, elastic, anisotropic and nearly incompressible hyperelastic materials. The diffusional expansion is available for this structural-diffusional analysis as a degree of freedom. To activate it we have to set the KEYOPT APDL parameter to 100001.

Creating Structural Geometries in ANSYS

Table 4.2: Nodes for Cube 1 (LCO)

node number	1	2	3	4	5	6	7	8
node location (X,Y,Z)	0,0,0	1,0,0	1,1,0	0,1,0	0,0,1	1,0,1	1,1,1	0,1,1

The model of these two materials was created using three cubes, two for LCO and one for PEO. To create each cube we used the same method as the previous model but with using 16 nodes instead of using the keypoints. Tables 4.2, 4.3 and 4.4, respectively,

Table 4.3: Nodes for Cube 2 (PEO)

node number	5	6	7	8	9	10	11	12
node location (X,Y,Z)	0,0,1	1,0,1	1,1,1	0,1,1	0,0,2	1,0,2	1,1,2	0,1,2

Table 4.4: Nodes for Cube 3 (LCO)

node number	9	10	11	12	13	14	15	16
node location (X,Y,Z)	0,0,2	1,0,2	1,1,2	0,1,2	0,0,3	1,0,3	1,1,3	0,1,3

show the nodes for the first, second and third cube. Selecting the nodes numbers from 1-8 and 9-16 to represent LCO material then define the nodes from 5-12 to represent PEO material. In order to change the thickness of PEO material, we have to change the Z location of the nodes 9-16. Figure 4.2 shows the sandwich LCO/PEO model.

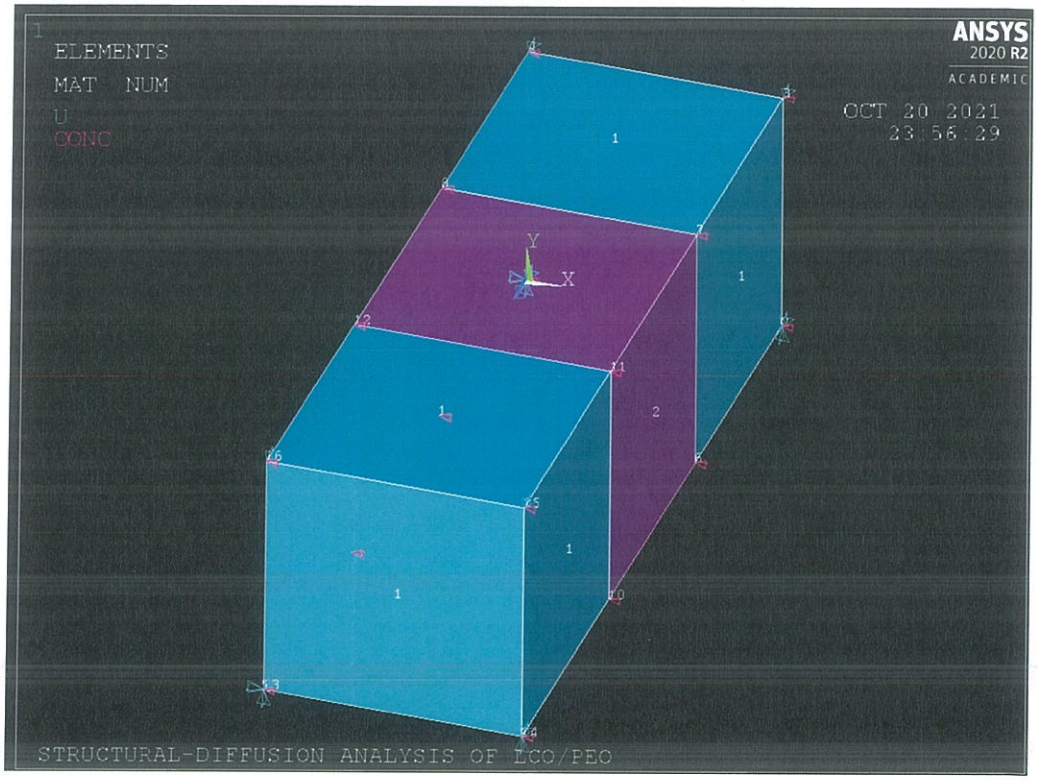

Figure 4.2: Structure of the sandwich LCO/PEO model showing node locations and applied loads.

Material Parameters and Properties

The LCO/PEO model is distinguished from the first PEO model by the existence of other type of applied strains. These strains are the chemical strains (diffusional lithiation strains) caused by the lithiation process. The cause of the chemical strains is the change in lithium concentration in the composite cathode material. The cathode will expand due to lithium intercalation, and shrink in the deintercalation. The total strain for the LCO is given by

$$\varepsilon_{ij} = \varepsilon_{ij}^{di} + \varepsilon_{ij}^{el} \tag{4.1}$$

where $\varepsilon_{ij} =$ total strains

$\varepsilon_{ij}^{di} =$ diffusional strain (chemical strains)

$\varepsilon_{ij}^{el} =$ elastic strain.

From Hook's law, we can write the elastic strain as

$$\varepsilon_{ij}^{el} = \frac{1}{E}(1+\nu)\sigma_{ij} - \nu\sigma_{kk}\delta_{ij} \tag{4.2}$$

where E : Young's modulus

σ_{ij} : stress

ν : Poisson's ratio

δ_{ij} : Kronecker delta.

The diffusional strain is given by

$$\varepsilon_{ij}^{di} = B_{ij} C_{sat} \triangle \overline{C} \tag{4.3}$$

where $\overline{C}$: Normalized concentration

B_{ij} : chemical expansion

C_{sat} : saturation concentration.

Since LCO exhibits anisotropic elastic material behaviour we have to use the components of the stiffness matrix as mentioned section 2.3.3 which we can activate by employ-

ing the ANEL command. For the chemical strains and material parameters for the half delithiated LCO we have to set the values for diffusion constants in Z direction saturation concentration as summarized in Table 4.5.

Table 4.5: LCO material parameters for diffusional expansion

Material parameter	APDL command	the value
Saturation concentration	CSAT	1
Reference concentration	CREF	0
Lithiation expansion coefficient in X direction	BETX	-0.0046
Lithiation expansion coefficient in Y direction	BETY	-0.0046
Lithiation expansion coefficient in Z direction	BETZ	0.048

Finally for PEO material properties we activate the data table TB, select the material number and element type and use the parameters or the constants in the USERMAT which are the Yong's modulus, Poisson's ratio and f interpolation parameter, and fill the stiffness matrix for LCO.

Loads and Boundary Conditions

There are two types of loads applied on this model. The displacement constraints or constrained degree of freedom in X,Y,Z directions, and the diffusional loads which are applied on the PEO material from LCO material. We have fixed the Z coordinates at the two outer surfaces 1,2,3,4 and 13,14,15,16 in order to confine the outer geometry in Z direction. To prevent any movements and rotations, we add constraints on nodes 1 and 3 and in Y direction and nodes 2 and 4 in X direction. In order to represent lithium concentration loads, we set all of the nodes to value 0.5.

4.3 Model 3: Realistic LCO/LLZ/PEO Cathode Microstructure

Element Types

For modeling the strains and stresses in the real microstructure of the composite cathode during lithiation and delithiation process, the structural-diffusion-thermal analysis was used with certain temperatures (273.15 K). For this model, three different element types were used to represent PEO, LCO and LLZ materials as these three materials have different behaviours. PEO exhibits a nonlinear hyperelastic response, whereas LCO is anisotropic elastic and LLZ is isotropic elastic.

Creating Structural Geometries in ANSYS

This model was built using GeoDict software as shown in Figure 4.3. The procedure for building this model was 1. piling process for LLZ fibers, these fibers were piled to be aligned horizontally in the XY plane and were 2. sintered afterwards. 3. The LLZ fibers were infiltrated with LCO particles. 4. PEO (or the binder) was added to the model. The final operation is the cropping of the microstructure as seen in Figure 4.4. To simulate this model in ANSYS, we use the Computational Geometry Algorithms Library (CGAL) 5.2 for meshing after the creation of the structure with GeoDict was completed.

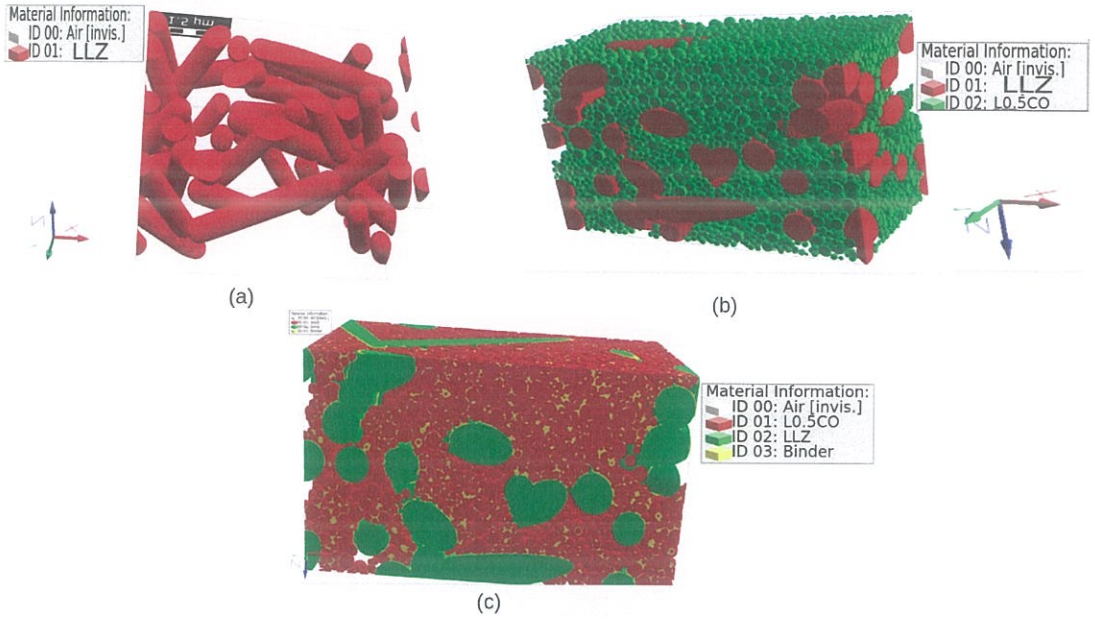

Figure 4.3: Building steps of the structural geometry of the realistic microstructure LCO/LLZ/PEO in GeoDict.

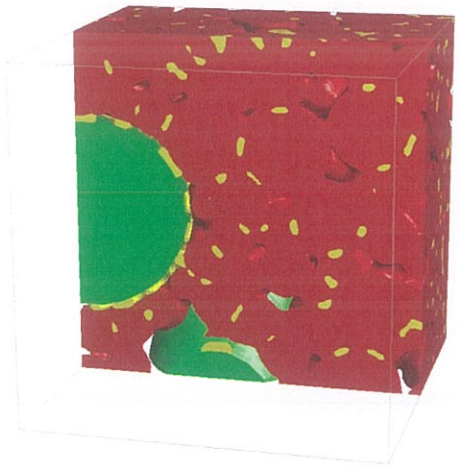

Figure 4.4: The final structural geometry for the realistic LCO/LLZ/PEO model.

Material Parameters and Properties

For this model, we define material properties as a constants or as a function of temperature for each material, activating the input table for LCO, PEO and LLZ. The material parameters for this model are given in Table 4.6. The elastic parameters of LCO are not defined in the table, because the anistropic elastic constants are defined from the stiffness

matrix which is the same as in the previous model.

Table 4.6: LCO/PEO/LLZ material parameters

Material parameter	APDL command	LCO value	LLZ value	PEO value
Elastic modulus	EX	-	146×10^9	100×10^6
Poisson's ratio	NUXY	-	0.26	0.4
Mass density	DENS	5050	5107	1000
Thermal expansion coefficients	CETX	-	0	0
Heat coefficient	CVH	100	100	100
Thermal conductivities	KXX	100	100	100
Specific heat	C	100	100	100

Chapter 5

Results and Discussion

5.1 Applying Uniaxial Loads in Simple PEO Model

After compiling the USERMAT with ANSYS 2020 R2 mechanical software and writing the APDL commands defining the required parameters, we simulate the nonlinear hyper-elastic material behaviour of the PEO cube under uniaxial tension and compression in the y direction with different values of displacement loads shown in Figure 5.1.

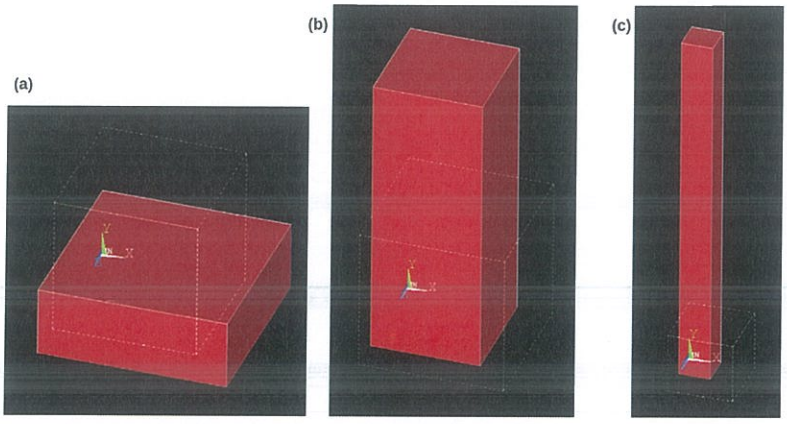

Figure 5.1: Uniaxial tension and compression in the simple PEO model with applied deformation gradient of (a) 0.5, (b) 2, and (c) 5.

5.1.1 The Effect of Changing the Parameter f

We studied the effect of varying the value of the interpolation parameter f from 0 to 1 on the shape of the stress-strain curve. For this we set the Poisson's ratio parameter (ν) to 0.4 and the Young's modulus to 10^8 Pa.

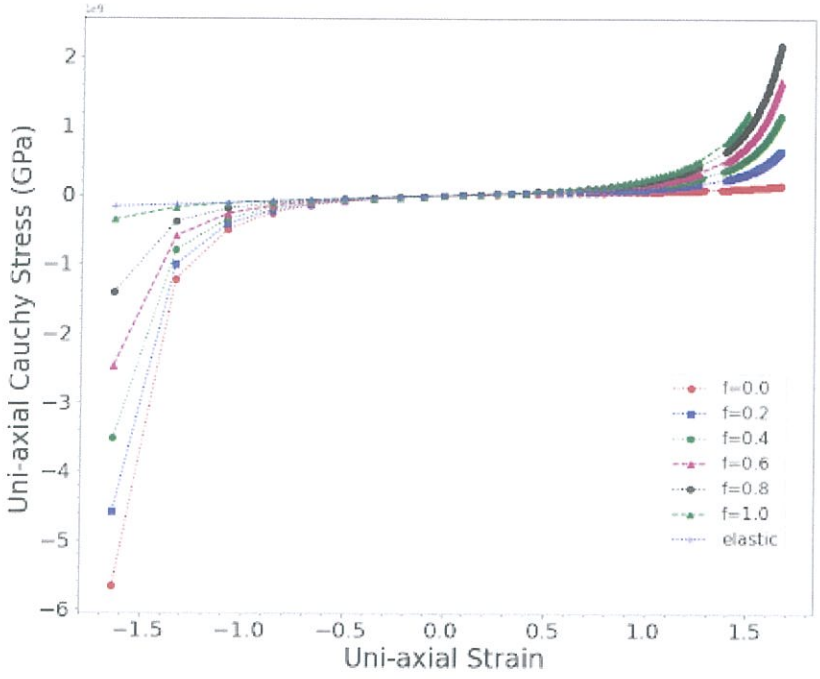

Figure 5.2: Stress strain results for different values of parameter f with strain range $[-2.0, 2.0]$.

Figures 5.3 and 5.2 show the effect of changing the parameter f. As shown in the figure, the behaviour for the same curve in tension case is different than the compressive case. In case of $f = 0.0$, for instance, we can notice the linear response in the tension case and a nonlinear with progressive response in the compressive case. Increasing the value of f leads to a more nonlinear response in the tension case and more less progressive in the compressive case. At $f = 0.5$ the curve is symmetric.

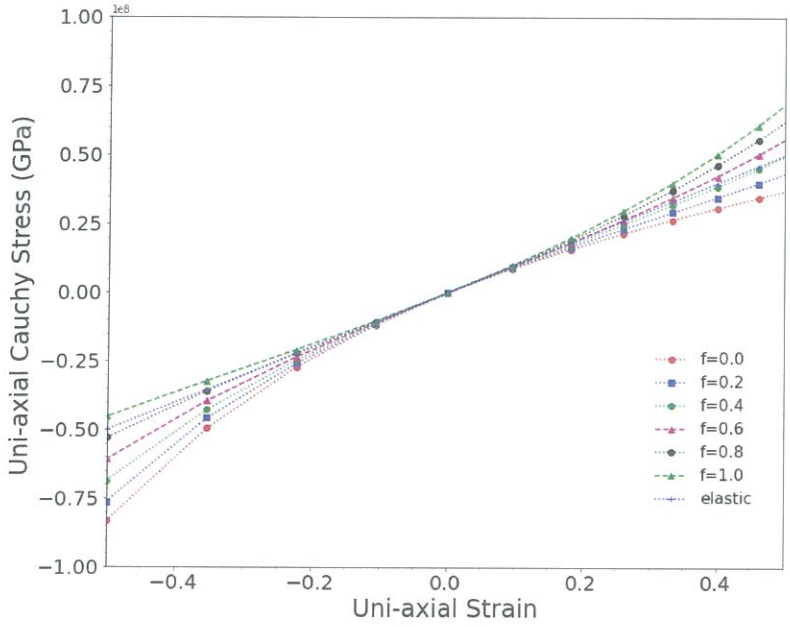

Figure 5.3: Stress strain results for different values of parameter f with strain range $[-0.5, 0.5]$.

5.1.2 Comparison with Previous Experimental Results

In order to decide which interpolation parameter f should be used in our next model (LCO/PEO), we compare our stress-strain curves with previous experimental results considering the same pure uniaxial tension and compression. The synthetic rubber neoprene material [8] showed a nonlinear stress-strain relationship in the experiment. The compressive and tensile parts are symmetric as shown in Figure 5.4. This symmetric behaviour corresponds to $f = 0.5$ in the Blatz-Ko model of Figure 5.5

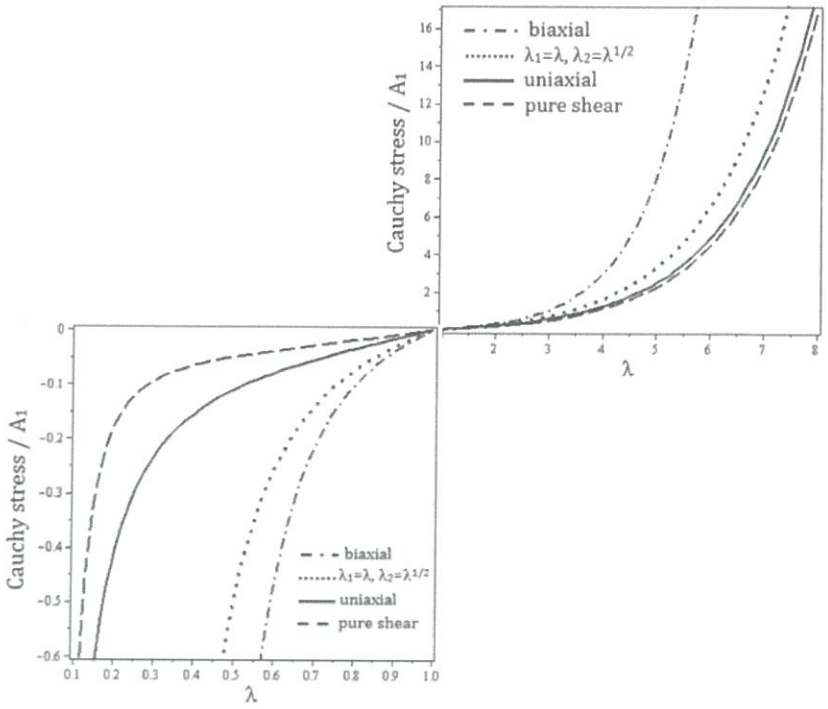

Figure 5.4: Experimental results for various tension and compression loading state.[8]

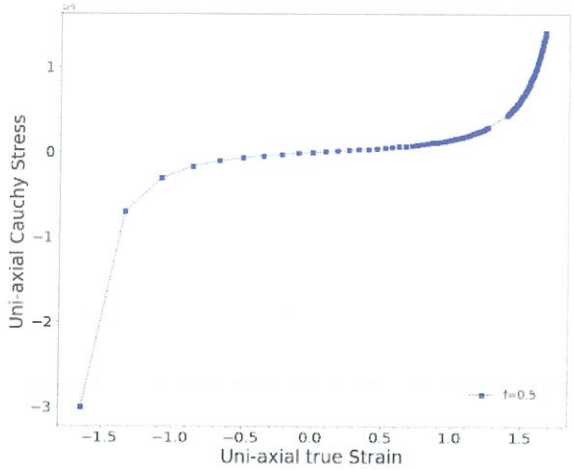

Figure 5.5: Stress-strain curve foruniaxial loading of Blatz-Ko model for f=0.5

5.1.3 Comparison between Elastic and Hyperelastic Model

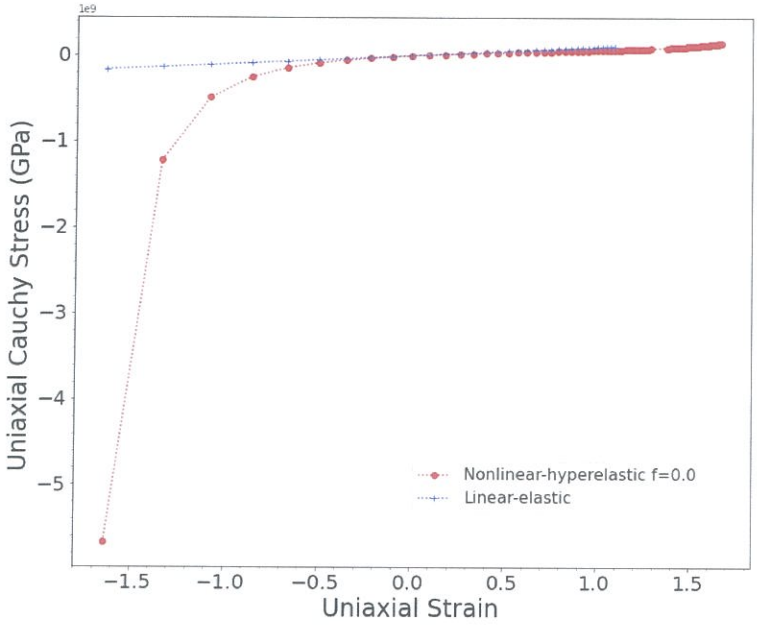

(a) With strain range (-2.0,2.0).

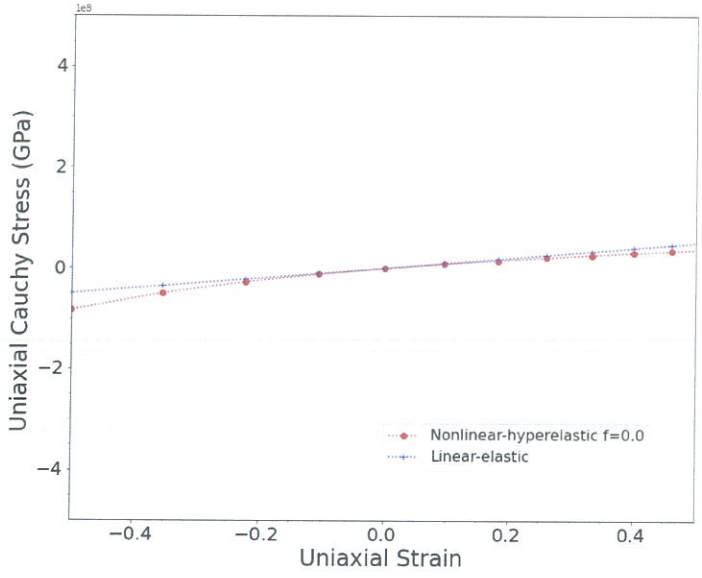

(b) with strain range (-0.5,0.5).

Figure 5.6: Comparison of the stress-strain curves of the linear elastic and the Blatz-Ko model with different strain ranges.

Figure 5.6 is presented for comparing between applying the large and the small strain theories on the PEO hyperelastic material behaviour of PEO. In the figure, we can notice the differences between the two curves. A nonlinear stress-strain curve was obtained by applying the large strain theory, and a linear stress-strain relation by applying the small strain theory. The stress values of the two models are equal for strain values between -0.2 and 0.2 since the stains are small for this period. Modeling the hyperelastic behaviour using the large strain theory for PEO shows that the stress values are more accurate and the material is more sensitive to larger strains in compression case.

5.2 Variation of PEO Thicknesses in the PEO/LCO Sandwich Model

To simulate both LCO and PEO material behaviours under the applied structural and chemical strains, we use our version of USERMAT to define the material properties of PEO, and we use the built-in anisotropic elastic model of ANSYS to define the material properties of LCO.

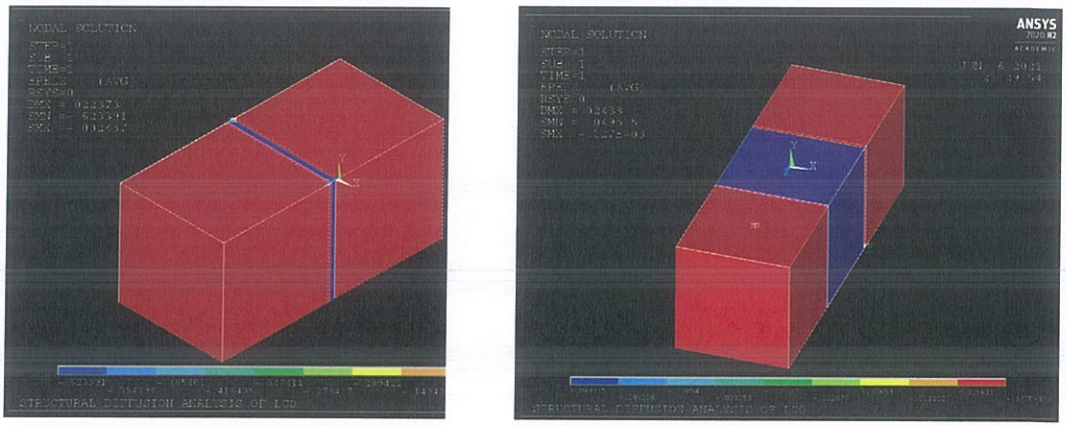

Figure 5.7: Geometry of the LCO/PEO model with different thicknesses for PEO

In order to see the effect of the structural-diffusional strains and the lithium concentration on PEO/LCO model results, we change the dimensions for the center cube (PEO), as Figure 5.7 shows, to control the thickness of PEO and obtain the corresponding results

for both stress and strain calculations.

5.2.1 Strain Results for PEO

The strain results for this model are the true strain, for activating this option we have to activate the non linearity solution or the large deformation option for the small strain theory calculation in ANSYS. By this, we can make a comparison between the strain results utilizing the small and the large strain theories as shown in Figure 5.8.

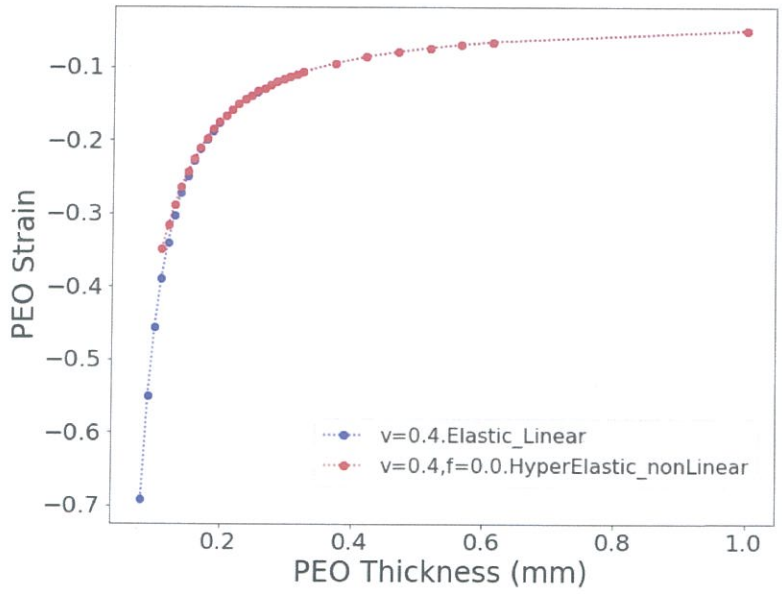

Figure 5.8: Strain-thickness curves of PEO/LCO model

5.2.2 Stress Results for PEO

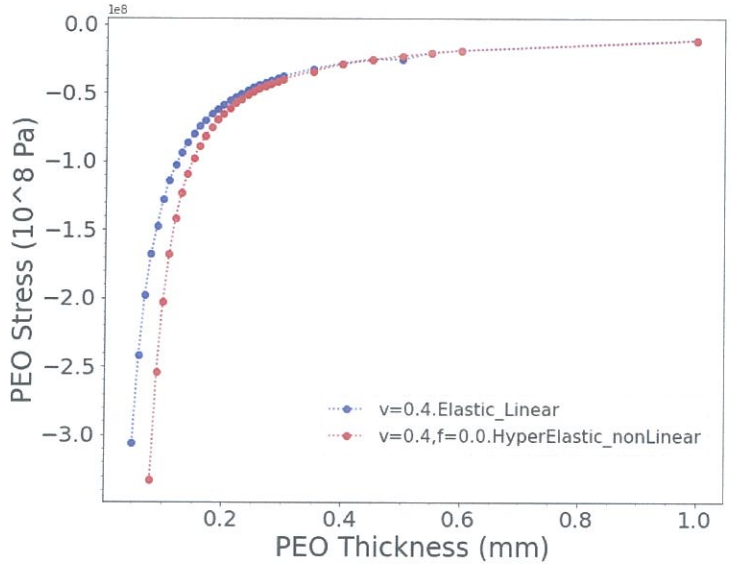

Figure 5.9: Stress-thickness curve for the PEO/LCO model.

Figure 5.9 shows the effect of changing the PEO thickness on the stress values. Two methods were applied to this model, the small and large strain theory to obtain the stress values for PEO model under the applied loads. The stress values for PEO will be equal to the average LCO stress values but of opposite sign.

The strain value is inversely proportional to the thickness of PEO. Therefore, the effect of applying the large strain theory will be more visible for smaller PEO thicknesses. By applying both large and small strain theories, we can notice that the stress results are almost the same for the PEO thickness values from 1 to 0.4 mm. The large strain theory is introducing a difference in this interval. On the other hand, for small PEO thickness values from 0.4 to 0.0 mm we can notice a difference between the two curves, because the applied displacements have more effect on the smaller thicknesses of PEO.

5.2.3 Stress-Strain Curves

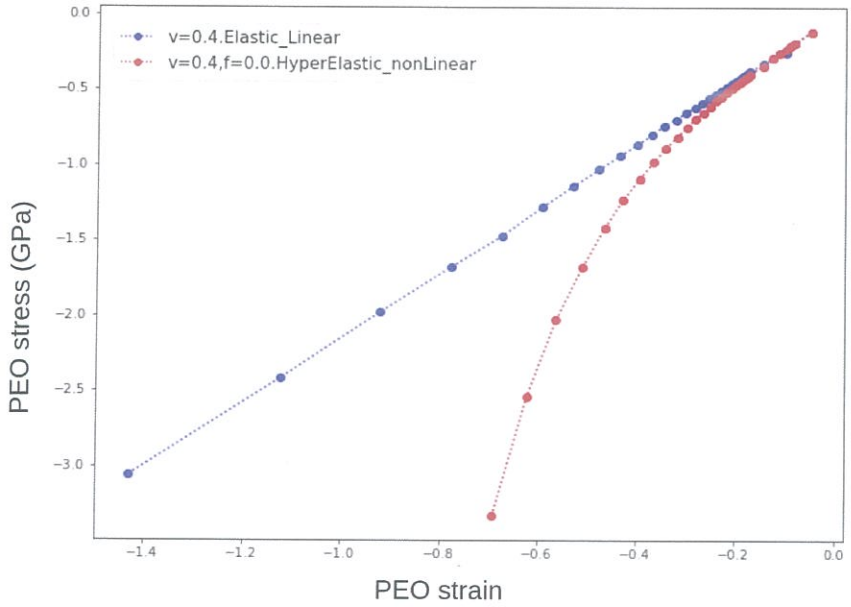

Figure 5.10: Stress-strain results in the PEO/LCO model

As shown in stress-strain curves of Figure 5.10, applying the large strain theory to study the material behaviour of PEO gave more accurate stress values than applying the small strain theory. We can conclude that the material is more sensitive at larger strains in this case. For the strain values < -0.2 (larger compression), we can notice the nonlinear stress-strain relationship in the curves of PEO.

5.3 ANSYS and GeoDict Results for Realistic Microstructure of the Composite Cathode

For this model GeoDict software was used to create the real microstructure for the composite cathode model. ANSYS software did not give a converged solution for this model due to the complexity of the geometry of this model or insufficient meshing. Therefore, the results from this software are not trusted. The following results are taken from GeoDict. Figure 5.11 shows the hyperelastic total strains; (b) ε_1 represent the first prin-

cipal strains as positive tensile strains; (b) ε_3 represent the third principal strains as negative compressive strains and (d) ε_{max} represents the maximum principal strains (principal strain with maximum absolute value).

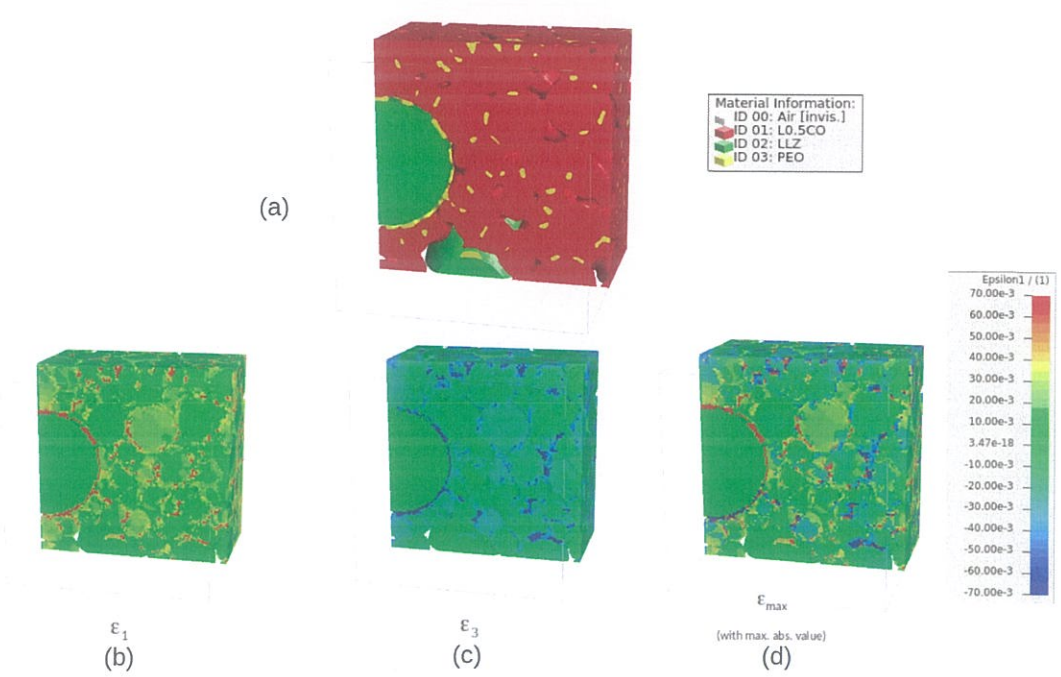

Figure 5.11: The figure (a) shows the microstructre of the realistic model and the bottom side shows the principal strain (hyperelastic strains), (b) ε_1, (c) ε_3, (d) ε_{max}.

5.3.1 Strain Results for Applying the Large and Small Strain Theories

Three different methods were used for the material behaviour of PEO in the composite cathode (LCO/PEO/LLZ): the small strain theory with the linear solution, large strain theory in elastic case and using the large strain theory.

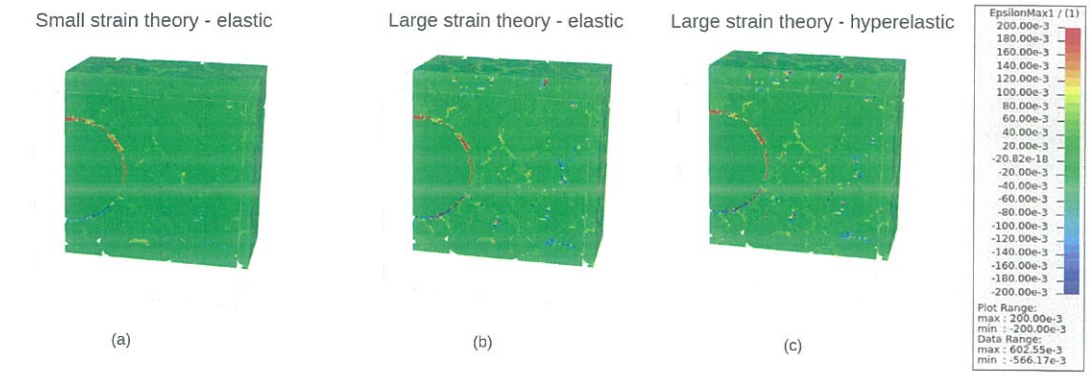

Figure 5.12: Strain results for the realistic microstructure model for applying different models

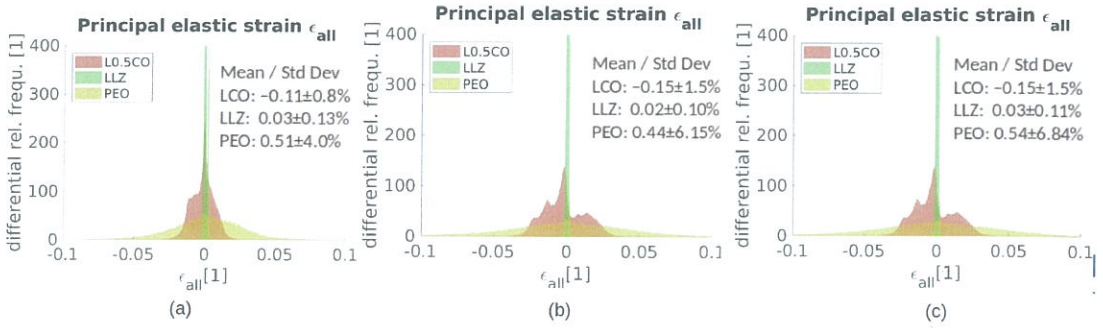

Figure 5.13: Histograms of Strain values for PEO, LCO and LLZ

Figure 5.13 shows the strain histograms for both of LCO, PEO and LLZ. Figure 5.13 (a) shows the results of applying the small strain theory. The mean values of strain results for PEO are 0.51% with standard deviation of 4%; for LCO are -0.11% with standard deviation 0.8% and for LLZ are 0.03% with standard deviation 0.13%. Figure 5.13 (b) shows the results of applying the small strain theory with the nonlinear solution. The mean values of the strain for PEO are 0.44% with standard deviation 6.15%; for LCO are -0.15% with standard deviation 1.5% and for LLZ are 0.02% with standard deviation 0.10%. Figure 5.13 (c) shows the results of applying the large strain theory. The mean values of the strain for PEO are 0.54% with standard deviation 6.84%, for LCO are -0.15 with standard deviation 1.5% and for LLZ are 0.03% with standard deviation 0.11%. We can notice that the width of LCO/LLZ distribution for the principal strains are similar for

applying the small theory. For the large strain theory, the width of the LCO/LLZ distribution is larger, but the width of the PEO strains distribution is the largest for applying the large strain theory.

5.3.2 Stress Results for Applying the Large and Small Strain Theories

We applied the same three calculation settings as the previous section to show the stress results for PEO in the realistic microstructural model.

Figure 5.14 shows the frequencies of the stress values for the three applied theories. Figure 5.14 (a) shows the results of applying the small strain theory. The mean values of the principal stress results for PEO are 3 MPa with standard deviation of 8 MPa.

Figure 5.14 (b) shows the results of applying the small strain theory with the nonlinear solution, the mean values of the principal stress results for PEO are 2 MPa with standard deviation of 11 MPa.

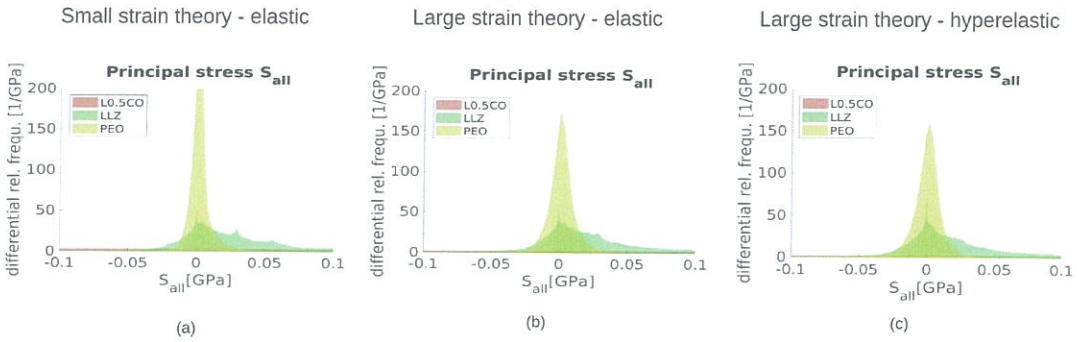

Figure 5.14: Histograms for the stress frequencies for PEO/LCO/LLZ model.

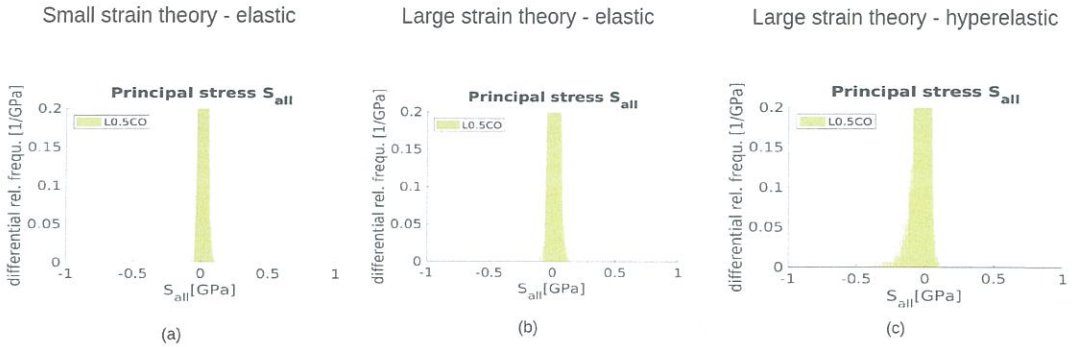

Figure 5.15: Detail view of stress distribution of PEO with visible changes in the width of the distribution.

Figure 5.14 (c) shows the results of applying the large strain theory, the mean values of principal stress results for PEO are -0.5 MPa with standard deviation of 19 MPa.

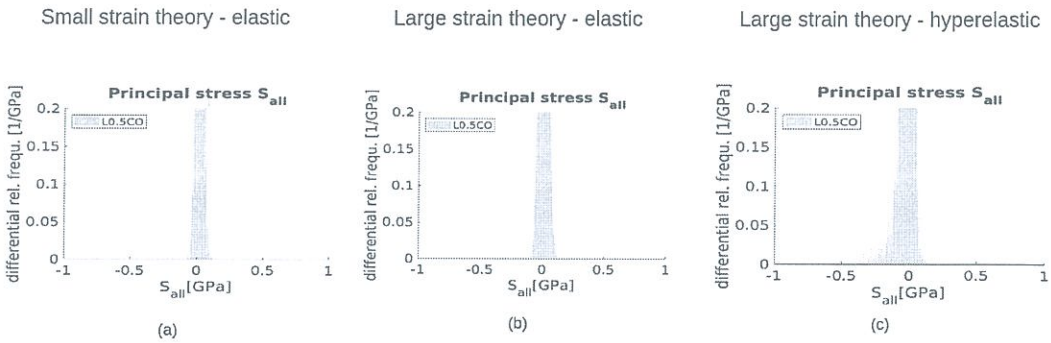

Figure 5.15: Detail view of stress distribution of PEO with visible changes in the width of the distribution.

Figure 5.14 (c) shows the results of applying the large strain theory, the mean values of principal stress results for PEO are -0.5 MPa with standard deviation of 19 MPa.

Chapter 6

Conclusions and Future Work

The composite cathode in all-solid-state lithium-ion batteries experiences an intensive deformation during the charging and discharging processes. Adding elastomers to the composite cathode material have proven to decrease the stresses in this process. In this work, the complicated hyperelastic nonlinear material behaviour of PEO using the large strain theory, specifically the Blatz and Ko model, was modeled in addition to the other two composite cathode materials LCO and LLZ to simulate the deformations that are occurring during the delithiation process. The finite element method and the finite volume method were used to simulate these deformations yielding the stress and strain distributions. The following points can be concluded.

- The spatial elasticity tensor or the stiffness matrix in the current configuration can be found and derived from the Cauchy stress directly without using the Piola transformation of the elasticity tensor.
- The nonlinear behaviour for the stress-strain curves for both the simple model and the LCO/PEO sandwich model demonstrates that the derived equations were successfully implemented.
- The difference in elastic (small large strain theory) and hyperelastic case was obvious and the hyperelastic stress results were more accurate for the simple models.

- In the realistic composite cathode model: PEO is affected most (10% change in strains, up-to 60% in stresses).

We are planning the following as future work.

- This model can be extended to simulate more complex behaviours like the viscoelastic or viscoplastic response in other applications (e.g. joints to compensate chemical expansions, dimension change during sintering).

- Find a novel method to develop the function of Blatz and Ko model as a decoupled function with both of isochoric and volumetric parts to improve the implementation of the viscoelastic material behaviour from this model.

- Make new studies to derive the Cauchy stress and elasticity tensors from the strain energy function (finding the spatial elasticity tensor directly from the Cauchy stress) as a function of the left Cauchy Green tensor (b). This would help to find direct relationship between the stress and strain in the large strain theory.

- Find the elasticity tensors for the anisotropic elastic materials with the calculations based on the Young's modulus and Poisson's ratio (Hooke's law). There is a direct relationship between the engineering stress and the engineering strain.

- Make improvements on the build-in ANSYS mechanical software to model the complex hyperelastic material behaviour for the generalised Blatz and Ko model by adding more freedom for selecting the interpolation parameter f and and Poisson's ratio ν.

Bibliography

[1] Y. Lyu, X. Wu, K. Wang, Z. Feng, T. Cheng, Y. Liu, M. Wang, R. Chen, L. Xu, J. Zhou, *et al.*, "An overview on the advances of $LiCoO_2$ cathodes for lithium-ion batteries," *Advanced Energy Materials*, vol. 11, no. 2, p. 2000982, 2021.

[2] S. Yamakawa, N. Nagasako, H. Yamasaki, T. Koyama, and R. Asahi, "Phase-field modeling of stress generation in polycrystalline $LiCoO_2$," *Solid State Ionics*, vol. 319, pp. 209–217, 2018.

[3] S. Shashkov and P. Dorozhkin, "AFM–raman characterization of li-ion batteries,"

[4] A. Mukhopadhyay and B. W. Sheldon, "Deformation and stress in electrode materials for li-ion batteries," *Progress in Materials Science*, vol. 63, pp. 58–116, 2014.

[5] H. Wang, Y.-I. Jang, B. Huang, D. R. Sadoway, and Y.-M. Chiang, "TEM study of electrochemical cycling-induced damage and disorder in $LiCoO_2$ cathodes for rechargeable lithium batteries," *Journal of the Electrochemical Society*, vol. 146, no. 2, p. 473, 1999.

[6] N. C. Rosero-Navarro, T. Kinoshita, A. Miura, M. Higuchi, and K. Tadanaga, "Effect of the binder content on the electrochemical performance of composite cathode using Li_6PS_5Cl precursor solution in an all-solid-state lithium battery," *Ionics*, vol. 23, no. 6, pp. 1619–1624, 2017.

[7] J. Wilmers and S. Bargmann, "A continuum mechanical model for the description of solvent induced swelling in polymeric glasses: Thermomechanics coupled with diffusion," *European Journal of Mechanics-A/Solids*, vol. 53, pp. 10–18, 2015.

[8] M. Mansouri and H. Darijani, "Constitutive modeling of isotropic hyperelastic materials in an exponential framework using a self-contained approach," *International Journal of Solids and Structures*, vol. 51, no. 25-26, pp. 4316–4326, 2014.

[9] F. Zheng, M. Kotobuki, S. Song, M. O. Lai, and L. Lu, "Review on solid electrolytes for all-solid-state lithium-ion batteries," *Journal of Power Sources*, vol. 389, pp. 198–213, 2018.

[10] A. Hadoush, "Finite element formulation of internally balanced blatz ko material model," vol. 14, pp. 215–221, 2020.

[11] S. A. Roberts, V. E. Brunini, K. N. Long, and A. M. Grillet, "A framework for three-dimensional mesoscale modeling of anisotropic swelling and mechanical deformation in lithium-ion electrodes," *Journal of The Electrochemical Society*, vol. 161, no. 11, p. F3052, 2014.

[12] Y. He, C. Lu, S. Liu, W. Zheng, and J. Luo, "Interfacial incompatibility and internal stresses in all-solid-state lithium ion batteries," *Advanced Energy Materials*, vol. 9, no. 36, p. 1901810, 2019.

[13] L. Wu, Y. Wen, and J. Zhang, "Three-dimensional finite element study on LI diffusion induced stress in FIB-SEM reconstructed $LiCoO_2$ half cell," *Electrochimica Acta*, vol. 222, pp. 814–820, 2016.

[14] S. Priyono, S. Hardiyani, N. Syarif, A. Subhan, and A. Suhandi, "Electrochemical performance of $LiMn_2O_4$ with varying thickness of cathode sheet," vol. 1191, no. 1, p. 012022, 2019.

[15] Y. Takahashi, N. Kijima, K. Dokko, M. Nishizawa, I. Uchida, and J. Akimoto, "Structure and electron density analysis of electrochemically and chemically delithiated $LiCoO_2$ single crystals," *Journal of Solid State Chemistry*, vol. 180, no. 1, pp. 313–321, 2007.

[16] R. Mücke, M. Finsterbusch, P. Kaghazchi, D. Fattakhova-Rohlfing, and O. Guillon, "Modelling electro-chemical induced stresses in all-solid-state batteries: Anisotropy effects in cathodes and cell design optimisation," *Journal of Power Sources*, vol. 489, p. 229430, 2021.

[17] H. Mendoza, S. A. Roberts, V. E. Brunini, and A. M. Grillet, "Mechanical and electrochemical response of a $LiCoO_2$ cathode using reconstructed microstructures," *Electrochimica Acta*, vol. 190, pp. 1–15, 2016.

[18] J. D. Gale, "Gulp: A computer program for the symmetry-adapted simulation of solids," *Journal of the Chemical Society, Faraday Transactions*, vol. 93, no. 4, pp. 629–637, 1997.

[19] F. Hart and J. Bates, "Lattice model calculation of the strain energy density and other properties of crystalline $LiCoO_2$," *Journal of Applied Physics*, vol. 83, no. 12, pp. 7560–7566, 1998.

[20] L. Wu and J. Zhang, "Ab initio study of anisotropic mechanical properties of $LiCoO_2$ during lithium intercalation and deintercalation process," *Journal of Applied Physics*, vol. 118, no. 22, p. 225101, 2015.

[21] O. L. Anderson, "A simplified method for calculating the debye temperature from elastic constants," *Journal of Physics and Chemistry of Solids*, vol. 24, no. 7, pp. 909–917, 1963.

[22] Y.-G. Lee, S. Fujiki, C. Jung, N. Suzuki, N. Yashiro, R. Omoda, D.-S. Ko, T. Shiratsuchi, T. Sugimoto, S. Ryu, *et al.*, "High-energy long-cycling all-solid-state lithium

metal batteries enabled by silver–carbon composite anodes," *Nature Energy*, vol. 5, no. 4, pp. 299–308, 2020.

[23] J. O. Besenhard, *Handbook of battery materials*. John Wiley & Sons, 2008.

[24] M. Moreno, R. Quijada, M. A. Santa Ana, E. Benavente, P. Gomez-Romero, and G. González, "Electrical and mechanical properties of poly (ethylene oxide)/intercalated clay polymer electrolyte," *Electrochimica Acta*, vol. 58, pp. 112–118, 2011.

[25] Z. Zhao, X. Mu, and F. Du, "Modeling and verification of a new hyperelastic model for rubber-like materials," *Mathematical Problems in Engineering*, vol. 2019, 2019.

[26] M. Hossain and P. Steinmann, "More hyperelastic models for rubber-like materials: consistent tangent operators and comparative study," *Journal of the Mechanical Behavior of Materials*, vol. 22, no. 1-2, pp. 27–50, 2013.

[27] B. Lin, "A new model for hyperelasticity," *Acta mechanica*, vol. 208, no. 1, pp. 39–53, 2009.

[28] K. Yaya and H. Bechir, "A new hyper-elastic model for predicting multi-axial behaviour of rubber-like materials: formulation and computational aspects," *Mechanics of Time-Dependent Materials*, vol. 22, no. 2, pp. 167–186, 2018.

[29] V. N. Khiêm and M. Itskov, "Analytical network-averaging of the tube model:: Rubber elasticity," *Journal of the Mechanics and Physics of Solids*, vol. 95, pp. 254–269, 2016.

[30] A. G. Holzapfel, *Nonlinear solid mechanics II*. John Wiley Sons, Inc., 2000.

[31] P. Velex, *International Gear Conference 2014: 26th-28th August 2014, Lyon*. Chandos Publishing, 2014.

[32] Y. Basar, D. Weichert, and J. Petrolito, "Nonlinear continuum mechanics of solids: Fundamental mathematical and physical concepts," *Appl. Mech. Rev.*, vol. 54, no. 6, pp. B98–B99, 2001.

Appendices

Appendix A

A.1 Mathematical Definitions

Kroneker delta :	$\delta_{ik} = \begin{cases} 1 & i = j \\ 0 & i \neq j \end{cases}$
Cayley-Hamilton equation:	$\mathbf{C}^3 + I_1 C^2 + I_2 C - I_3 \mathbf{I} = 0$
Trace of $n \times n$ matrix $\mathbf{C}$	$tr(C) = \sum = c_{ii}$
The second invariant $\mathrm{I}_2(C) = \frac{1}{2}[(tr(C))^2 - tr(C^2)]$	$= C_{ii}C_{jj} - C_{ji}C_{ij} = trC^{-1} detC$
Identity matrix in fourth order tensor	$\mathbb{I} = \delta_{ij}\delta_{kl} e_i \otimes e_k \otimes e_l \otimes e_k$
The dyadic product operator	$\mathbb{I} \otimes \mathbb{I} = \delta_{ij}\delta_{kl}$
The operator $\odot$ is defined as	$\mathbb{I} \odot \mathbb{I} = \delta_{ik}\delta_{il} + \delta_{il}\delta_{jk}$
Derivative of $\mathbf{C}^{-1}$ with respect to $\mathbf{C}$	$-\frac{\partial \mathbf{C}^{-1}}{\partial \mathbf{C}} = \mathbf{C}^{-1} \odot \mathbf{C}^{-1}$
Derivative of $\mathbf{C}^{-2}$ with respect to $\mathbf{C}$	$-\frac{\partial \mathbf{C}^{-2}}{\partial \mathbf{C}} = \mathbf{C}^{-2} \odot \mathbf{C}^{-1} + \mathbf{C}^{-1} \odot \mathbf{C}^{-2}$

A.2 ANSYS Parametric Design Language (APDL) Codes

A.2.1 APDL Code for Simple PEO Model Structure

```
1 FINISH
2 /CLEAR, START, NEW
3 /batch,list
4 /title, PEO simple case
5 /com, uniaxial tension stress, large deformation.
```

```
/com,
/prep7
ele1=185
mat1=1
et,1,ele1
mat,mat1
k,1,0,0,0
k,2,1,0,0
k,3,1,0,1
k,4,0,0,1
k,5,0,1,0
k,6,1,1,0
k,7,1,1,1
k,8,0,1,1
a,1,2,3,4
a,1,4,8,5
a,1,2,6,5
a,2,3,7,6
a,3,4,8,7
a,5,6,7,8
va,1,2,3,4,5,6
esize,1
et,1,185
vmesh,all
elist
da,6,uy,5
da,1,uy,0
dk,1,ux,0
dk,1,uy,0
dk,1,uz,0
dk,4,ux,0
nlgeom,on
tb,user,mat1,1,1
tbdata,mat1,100e6,0.4,0.5
eplot
nlgeom,on
eplot
/solve
solve
fini
/post26
```

A.2.2 LCO/PEO model

```
FINISH
/CLEAR, START, NEW
/TITLE, STRUCTURAL-DIFFUSION ANALYSIS OF LCO/PEO
/nopr
/PREP7
ele1=226
mat1=1
N,1,0,0,0
N,2,1,0,0
N,3,1,1,0
N,4,0,1,0
N,5,0,0,1
N,6,1,0,1
N,7,1,1,1
N,8,0,1,1
N,9,0,0,2
N,10,1,0,2
N,11,1,1,2
N,12,0,1,2
N,13,0,0,3
N,14,1,0,3
N,15,1,1,3
N,16,0,1,3
MAT,1
ET,1,226
E,1,2,3,4,5,6,7,8
E,9,10,11,12,13,14,15,16
ET,1,226,100001
TB,ANEL,1,,1
TBDATA,1,303.86E9,100.71E9,32.58E9,0.,7.31E9,0.
TBDATA,7,318.93E9,28.66E9,0.,-3.93E9,0.,98.93E9
TBDATA,13,0.,7.03E9,0.,18.02E9,0.,-2.46E9.
TBDATA,19,15.73E9,0.,101.94E9

MP,BETZ,1,0.048
MP,BETX,1,-0.0046
MP,BETY,1,-0.0046
MP,CSAT,1,1
MP,CREF,1,0
D,all,CONC,0.5
ele2=185
mat2=2
MAT,2
```

```
ET,2,185
E,5,6,7,8,9,10,11,12
tb,user,2
tbdata,2,100e6
D,1,UZ,0
D,2,UZ,0
D,3,UZ,0
D,4,UZ,0
D,13,UZ,0
D,14,UZ,0
D,15,UZ,0
D,16,UZ,0
D,1,UX,0
D,1,UY,0
D,2,UY,0
D,13,UX,0
D,13,UY,0
D,14,UY,0
D,all,CONC,0.5

nlgeom,on

/solve
solve
eplot
/solve
```

A.2.3 Realistic LCO/LLZ/PEO cathode microstructure

```
Realistic LCO/LLZ/PEO cathode microstructure

/PREP7

/UNITS,SI
CSYS,0
TOFFST,273.15
TREF,0

#LCO
MP,DENS,1,5050
TB,ANEL,1,,1
TBDATA,1,303.86E9,100.71E9,32.58E9,0.,7.31E9,0.
```

```
TBDATA,7,318.93E9,28.66E9,0.,-3.93E9,0.,98.93E9
TBDATA,13,0.,7.03E9,0.,18.02E9,0.,-2.46E9.
TBDATA,19,15.73E9,0.,101.94E9


MP,CTEX,1,6.67e-5
MP,KXX,1,100
MP,C,1,100
MP,CVH,1,100

#LLZ
MP,DENS,2,5107
MP,EX,2,146E+09
MP,NUXY,2,0.26
MP,CTEX,2,0
MP,KXX,2,100
MP,C,2,100
MP,CVH,2,100

#PEO
MP,DENS,3,1000
tb,user,3,,
tbdata,1,100e6,0.4,0.0
MP,CTEX,3,0
MP,KXX,3,100
MP,C,3,100
MP,CVH,3,100
```

A.3 USERMAT

```
      subroutine usermat3d(
     &                     matId, elemId,kDomIntPt, kLayer, kSectPt,
     &                     ldstep,isubst,keycut,
     &                     nDirect,nShear,ncomp,nStatev,nProp,
     &                     Time,dTime,Temp,dTemp,
     &                     stress,ustatev,dsdePl,sedEl,sedPl,epseq,
     &                     Strain,dStrain, epsPl, prop, coords,
     &                     var0, defGrad_t, defGrad,
     &                     tsstif, epsZZ,
     &                     var1, var2, var3, var4, var5,
     &                     var6, var7, var8)
C
```

```
c     input arguments
c     ===============
c      matId      (int,sc,i)              material no.
c      elemId     (int,sc,i)              element no.
c      kDomIntPt  (int,sc,i)              "k"th domain integration point
c      kLayer     (int,sc,i)              "k"th layer
c      kSectPt    (int,sc,i)              "k"th Section point
c      ldstep     (int,sc,i)              load step number
c      isubst     (int,sc,i)              substep number
c      nDirect    (int,sc,in)             no. of direct components
c      nShear     (int,sc,in)             no. of shear components
c      ncomp      (int,sc,in)             nDirect + nShear
c      nstatev    (int,sc,1)              Number of state variables
c      nProp      (int,sc,1)              Number of material ocnstants
c
c      Temp       (dp,sc,in)              temperature at beginning of
c                                         time increment
c      dTemp      (dp,sc,in)              temperature increment
c      Time       (dp,sc,in)              time at beginning of increment (t)
c      dTime      (dp,sc,in)              current time increment (dt)
c
c      Strain    (dp,ar(ncomp),i)         Strain at beginning of time increment
c      dStrain   (dp,ar(ncomp),i)         Strain increment
c      prop      (dp,ar(nprop),i)         Material constants defined by TB,USER
c      coords    (dp,ar(3),i)             current coordinates
c      defGrad_t(dp,ar(3,3),i)            Deformation gradient at time t
c      defGrad   (dp,ar(3,3),i)           Deformation gradient at time t+dt
c
c     input output arguments
c     ======================
c      stress    (dp,ar(nTesn),io)        stress
c      ustatev    (dp,ar(nstatev),io)     user state variable
c            ustatev(1)                     - equivalent plastic strain
c            ustatev(2) - statev(1+ncomp)   - plastic strain vector
c            ustatev(nStatev)               - von-Mises stress
c      sedEl     (dp,sc,io)               elastic work
c      sedPl     (dp,sc,io)               plastic work
c      epseq     (dp,sc,io)               equivalent plastic strain
c      tsstif    (dp,ar(2),io)            transverse shear stiffness
c                                         tsstif(1) - Gxz
c                                         tsstif(2) - Gyz
c                                         tsstif(1) is also used to       c
c                                         hourglass
c                                         stiffness, this value must be   c
c                                         order element, such as 181,
c                                         182, 185 with uniform
```

```
c                                          integration is used.
c      var no.      (dp,sc,io)                 not used, they are reserved arguments
c                                          for further development
c
c     output arguments
c     ================
c      keycut    (int,sc,io)               loading bisect/cut control
c                                          0 - no bisect/cut
c                                          1 - bisect/cut
c                                          (factor will be determined
c                                          by ANSYS solution control)
c     dsdeEl    (dp,ar(ncomp,ncomp),io)    material jacobian matrix
c      epsZZ     (dp,sc,o)                 strain epsZZ for plane stress,
c                                          define it when accounting
c                                          for thickness change
c                                          in shell and plane stress states
c
c*************************************************************************
c
c      ncomp   6   for 3D  (nshear=3)
c      ncomp   4   for plane strain or axisymmetric (nShear = 1)
c      ncomp   3   for plane stress (nShear = 1)
c      ncomp   3   for 3d beam      (nShear = 2)
c      ncomp   1   for 1D (nShear = 0)
c
c      stresss and strains, plastic strain vectors
c          11, 22, 33, 12, 23, 13    for 3D
c          11, 22, 33, 12            for plane strain or axisymmetry
c          11, 22, 12                for plane stress
c          11, 13, 12                for 3d beam
c          11                        for 1D
c
c      material jacobian matrix
c        3D
c          dsdeEl      1111   1122   1133   1112   1123   1113
c          dsdeEl      2211   2222   2233   2212   2223   2213
c          dsdeEl      3311   3322   3333   3312   3323   3313
c          dsdeEl      1211   1222   1233   1212   1223   1213
c          dsdeEl      2311   2322   2333   2312   2323   2313
c          dsdeEl      1311   1322   1333   1312   1323   1313
c        plane strain or axisymmetric (11, 22, 33, 12)
c          dsdeEl      1111   1122   1133   1112
c          dsdeEl      2211   2222   2233   2212
c          dsdeEl      3311   3322   3333   3312
c          dsdeEl      1211   1222   1233   1212
c        plane stress (11, 22, 12)
```

```
105 c           dsdeEl       1111   1122   1112
106 c           dsdeEl       2211   2222   2212
107 c           dsdeEl       1211   1222   1212
108 c         3d beam (11, 13, 12)
109 c           dsdeEl       1111   1113   1112
110 c           dsdeEl       1311   1313   1312
111 c           dsdeEl       1211   1213   1212
112 c         1d
113 c           dsdeEl       1111
114 c
115 c*************************************************************************
116 #include "impcom.inc"
117 c include "ansysdef.inc"
118 c
119       INTEGER
120      &                 matId, elemId,
121      &                 kDomIntPt, kLayer, kSectPt,
122      &                 ldstep,isubst,keycut,
123      &                 nDirect,nShear,ncomp,nStatev,nProp
124             INTEGER          matId,elemId, kDomIntPt,kLayer,kSectPt,ldstep,
125      &                 isubst,keycut, nDirect,nShear,ncomp,nStatev,nProp
126       DOUBLE PRECISION
127      &                 Time,    dTime,   Temp,    dTemp,
128      &                 sedEl,   sedPl,   epseq,   epsZZ,   cutFactor
129       DOUBLE PRECISION
130      &                 stress  (ncomp  ), ustatev (nStatev),
131      &                 dsdePl  (ncomp,ncomp),        dsdeEl  (ncomp,ncomp),
132      &                 Strain  (ncomp  ), dStrain (ncomp  ),
133      &                 epsPl   (ncomp  ), prop (nProp  ),
134      &                 coords  (3), defGrad (3,3), defGrad_t(3,3),
135      &                 tsstif  (2),  BLCG(6), BLCGINV(6),
136      &                 defGradINV(3,3)
137 cc
138 c     DOUBLE PRECISION Time,dTime,Temp,dTemp,sedEl,sedPl,epseq,epsZZ
139 c      DOUBLE PRECISION stress  (ncomp  ),ustatev (nStatev),
140 c     &   dsdePl  (ncomp,ncomp), dsdeEl  (ncomp,ncomp),
141 c     &   Strain  (ncomp  ),dStrain (ncomp  ),
142 c     &   epsPl   (ncomp  ),prop    (nProp  ),coords  (3),defGrad (3,3),
143 c     &   defGrad_t(3,3),tsstif  (2),BLCG(6),EELAS(6),CRCG(6)
144 c
145 c***************** User defined part **************************
146 c
147 c --- parameters
148
149       integer          mcomp
150       double precision HALF,THIRD,ONE,TWO,SMALL,ONEHALF,ZERO,TWOTHIRD,
```

```
151       &    ONEDM02,ONEDM05,sqTiny
152        parameter        (ZERO       = 0.d0,HALF       = 0.5d0,
153       &    THIRD       = 1.d0/3.d0,ONE         = 1.d0,TWO        = 2.d0,
154       &    SMALL       = 1.d-08,sqTiny     = 1.d-20,ONEDM02    = 1.d-02,
155       &    ONEDM05     = 1.d-05,ONEHALF    = 1.5d0,
156       &    TWOTHIRD    = 2.0d0/3.0d0)
157  c
158  c --- local variables
159  c
160  c       sigElp    (dp,ar(6  ),1)           trial stress
161  c       dsdeEl    (dp,ar(6,6),1)           elastic moduli
162  c       sigDev    (dp,ar(6  ),1)           deviatoric stress tensor
163  c       dfds      (dp,ar(6  ),1)           derivative of the yield function
164  c       JM        (dp,ar(6,6),1)           2D matrix for a 4 order tensor
165  c       pEl       (dp,sc     ,1)           hydrostatic pressure stress
166  c       qEl       (dp,sc     ,1)           von-mises stress
167  c       pleq_t    (dp,sc     ,1)           equivalent plastic strain at beginning
168                                             of time increment
169  c       pleq      (dp,sc     ,1)           equivalent plastic strain at end
170                                             of time increment
171  c       dpleq     (dp,sc     ,1)           incremental equivalent plastic strain
172  c       sigy_t    (dp,sc     ,1)           yield stress at beginning of
173                                             time increments
174  c       sigy      (dp,sc     ,1)           yield stress at end of
175                                             time increment
176  c       young     (dp,sc     ,1)           Young's modulus
177  c       posn      (dp,sc     ,1)           Poisson's ratio
178  c       sigy0     (dp,sc     ,1)           initial yield stress
179  c       dsigdep   (dp,sc     ,1)           plastic slop
180  c       twoG      (dp,sc     ,1)           two time of shear moduli
181  c       threeG    (dp,sc     ,1)           three time of shear moduli
182  c
183  c --- temperary variables for solution purpose
184  c       i, j
185  c       threeOv2qEl, oneOv3G, qElOv3G, con1, con2, fratio
186  c
187        EXTERNAL          vzero,vmove,get_ElmData
188        double precision sigElp(ncomp),G(ncomp),
189       &    sigDev(ncomp),JM     (ncomp,ncomp),dfds(ncomp),sigi  (ncomp),
190       &    strainEl(ncomp)
191
192        double precision var0,var1,var2,var3,var4,var5,var6,var7,var8
193
194  c       DATA G/1.0D0,1.0D0,1.0D0,0.0D0,0.0D0,0.0D0/
195  c
196        integer           i,j
```

```
197       double precision pEl,qEl,pleq_t,sigy_t ,sigy,dpleq,pleq,young,
198      &   posn,sigy0,dsigdep,elast1,elast2,twoG,threeG,oneOv3G,qElOv3G,
199      &   threeOv2qEl,fratio,con1,con2,dperr(3),
200      &   M,N,DET,INVDET,B,f,poissonsratio
201     c**********************************************************************
202
203
204
205
206     C ----------------------------------------------------------------
207
208     C BLCG -  LEFT CAUCHY-GREEN TENSOR
209     C defGrad - DEFORMATION GRADIENT
210     C ----------------------------------------------------------------
211
212       young    = prop(1)
213       poissonsratio = prop(2)
214       f = prop(3)
215       B = poissonsratio/(1-(2*poissonsratio))
216       M     = young /(2*(1+ poissonsratio))
217       tsstif(1) = M
218       ustatev(1)= 0.0
219       pleq_t   = ustatev(1)
220       pleq     = pleq_t
221
222       DET=defGrad(1,1)*defGrad(2,2)*defGrad(3,3)-defGrad(1,2)
223      & *defGrad(2,1)*defGrad(3,3)
224         DET=DET+defGrad(1,2)*defGrad(2,3)*defGrad(3,1)+defGrad(1,3)
225      & *defGrad(3,2)*defGrad(2,1)-defGrad(1,3)*defGrad(3,1)*defGrad(2,2)
226      & -defGrad(2,3)*defGrad(3,2)*defGrad(1,1)
227
228         DO i=1,3
229                 print *, 'F ', defGrad(i,:)
230         END DO
231
232         print *, 'Det ', DET
233
234
235         BLCG(1)=defGrad(1,1)**2+defGrad(1,2)**2+defGrad(1,3)**2
236         BLCG(2)=defGrad(2,1)**2+defGrad(2,2)**2+defGrad(2,3)**2
237         BLCG(3)=defGrad(3,3)**2+defGrad(3,1)**2+defGrad(3,2)**2
238         BLCG(4)=defGrad(1,1)*defGrad(2,1)+defGrad(1,2)*defGrad(2,2)
239      &    +defGrad(1,3)*defGrad(2,3)
240
241            BLCG(6)=defGrad(1,1)*defGrad(3,1)+defGrad(1,2)*defGrad(3,2)
242      &    +defGrad(1,3)*defGrad(3,3)
```

```
243         BLCG(5)=defGrad(2,1)*defGrad(3,1)+defGrad(2,2)*defGrad(3,2)
244      &   +defGrad(2,3)*defGrad(3,3)
245        DO i=1,ncomp
246                 print *, 'B ', BLCG(i)
247        END DO
248
249
250
251
252        INVDET=1/DET
253
254        defGradINV(1,1) = +(INVDET) * (defGrad(2,2)*defGrad(3,3) -
255      &          defGrad(2,3)*defGrad(3,2))
256        defGradINV(2,1) = -(INVDET) * (defGrad(2,1)*defGrad(3,3) -
257      &          defGrad(2,3)*defGrad(3,1))
258        defGradINV(3,1) = +(INVDET) * (defGrad(2,1)*defGrad(3,2) -
259      &          defGrad(2,2)*defGrad(3,1))
260        defGradINV(1,2) = -(INVDET) * (defGrad(1,2)*defGrad(3,3) -
261      &          defGrad(1,3)*defGrad(3,2))
262        defGradINV(2,2) = +(INVDET )* (defGrad(1,1)*defGrad(3,3) -
263      &          defGrad(1,3)*defGrad(3,1))
264        defGradINV(3,2) = -(INVDET) * (defGrad(1,1)*defGrad(3,2) -
265      &          defGrad(1,2)*defGrad(3,1))
266        defGradINV(1,3) = +(INVDET)* (defGrad(1,2)*defGrad(2,3) -
267      &          defGrad(1,3)*defGrad(2,2))
268        defGradINV(2,3) = -(INVDET) * (defGrad(1,1)*defGrad(2,3) -
269      &          defGrad(1,3)*defGrad(2,1))
270        defGradINV(3,3) = +(INVDET) * (defGrad(1,1)*defGrad(2,2) -
271      &          defGrad(1,2)*defGrad(2,1))
272          DO i=1,3
273                       print *, 'invdef ', defGradINV(i,:)
274          END DO
275
276
277        BLCGINV(1)=defGradINV(1,1)**2+defGradINV(2,1)**2+
278      &    defGradINV(3,1)**2
279        BLCGINV(2)=defGradINV(1,2)**2+defGradINV(2,2)**2+
280      &    defGradINV(3,2)**2
281        BLCGINV(3)=defGradINV(3,3)**2+defGradINV(1,3)**2+
282      &    defGradINV(2,3)**2
283        BLCGINV(4)=defGradINV(1,1)*defGradINV(1,2)+defGradINV(2,1)*
284      &    defGradINV(2,2)+defGradINV(3,1)*defGradINV(3,2)
285        BLCGINV(6)=defGradINV(1,1)*defGradINV(1,3)+defGradINV(2,1)*
286      &    defGradINV(2,3)+defGradINV(3,1)*defGradINV(3,3)
287        BLCGINV(5)=defGradINV(1,2)*defGradINV(1,3)+defGradINV(2,2)*
288      &    defGradINV(2,3)+defGradINV(3,2)*defGradINV(3,3)
```

```
289
290         DO i=1,ncomp
291                 print *, 'BINV ', BLCGINV(i)
292         END DO
293
294
295
296   C  CALCULATE THE STRESS(Cauchy Stress)
297
298        INVDET=1/DET
299        N=M*INVDET
300
301        DO i=1,3
302          stress(i)=N*(1-f)*(DET**(2*B)-BLCGINV(i)) +
303       &    N*f*(BLCG(i)-INVDET**(2*B))
304        END DO
305        DO i=4,6
306          stress(i)=N*((f*BLCG(i))-((1-f)* BLCGINV(i)))
307        END DO
308
309          DO i=1,ncomp
310                  print *, 'stress ', stress(i)
311          END DO
312
313
314
315   c**** Update the Plastic work
316
317        DO i = 1 , nDirect
318           epsPl(i) = 0.0
319        END DO
320        DO i = nDirect + 1 , ncomp
321           epsPl(i) = 0.0
322        END DO
323        epseq  = pleq
324
325
326        ustatev(1) = pleq
327        do i=1,ncomp
328           ustatev(i+1) = epsPl(i)
329        end do
330
331
332   c**** Update the elastic work
333        sedEl = ZERO
334        DO i = 1 , ncomp
```

```
335           sedEl = sedEl + stress(i)*(Strain(i)+dStrain(i))
336         END DO
337
338   c CALCULATE THE JACOBIAN MATRIX(D)
339
340           DO i=1,6
341             DO j=1,6
342               dsdePl(i,j)=0.0
343             END DO
344           END DO
345
346           dsdePl(1,1)=N*(f*(2*B+2)*(INVDET**(2*B))+
347          &          (1-f)*(2*B-2)*DET**(2*B)+ 4*(1-f)*BLCGINV(1))
348           dsdePl(2,2)=N*(f*(2*B+2)*(INVDET**(2*B))+
349          &          (1-f)*(2*B-2)*DET**(2*B)+ 4*(1-f)*BLCGINV(2))
350           dsdePl(3,3)=N*(f*(2*B+2)*(INVDET**(2*B))+
351          &          (1-f)*(2*B-2)*DET**(2*B)+ 4*(1-f)*BLCGINV(3))
352           dsdePl(4,4)=N*(f*(INVDET**(2*B))-(1-f)*DET**(2*B)+
353          &          (1-f)*BLCGINV(1)+BLCGINV(2))
354           dsdePl(5,5)=N*(f*(INVDET**(2*B))-(1-f)*DET**(2*B)+
355          &    (1-f)*BLCGINV(2)+BLCGINV(3))
356           dsdePl(6,6)=N*(f*(INVDET**(2*B))-(1-f)*DET**(2*B)+
357          &    (1-f)*BLCGINV(1)+BLCGINV(3))
358           dsdePl(1,2)=N*(f*(2*B)*(INVDET**(2*B))+
359          &          (1-f)*(2*B)*DET**(2*B)
360           dsdePl(1,3)=N*(f*(2*B)*(INVDET**(2*B))+
361          &          (1-f)*(2*B)*DET**(2*B)
362           dsdePl(2,3)=N*(f*(2*B)*(INVDET**(2*B))+
363          &   (1-f)*(2*B)*DET**(2*B)
364           dsdePl(1,4)=2*N*(1-f)*BLCGINV(4)
365           dsdePl(1,5)=0.0
366           dsdePl(1,6)=2*N*(1-f)*BLCGINV(6)
367           dsdePl(2,4)=2*N*(1-f)*BLCGINV(4)
368           dsdePl(2,5)=2*N*(1-f)*BLCGINV(5)
369           dsdePl(2,6)=0.0
370           dsdePl(3,4)=0.0
371           dsdePl(3,5)=2*N*(1-f)*BLCGINV(5)
372           dsdePl(3,6)=2*N*(1-f)*BLCGINV(6)
373           dsdePl(4,5)=N*(1-f)*BLCGINV(6)
374           dsdePl(4,6)=N*(1-f)*BLCGINV(5)
375           dsdePl(5,6)=N*(1-f)*BLCGINV(4)
376           DO i=1,ncomp-1
377                   DO j=i+1,ncomp
378                           dsdePl(j,i)=dsdePl(i,j)
379                   END DO
380         END DO
```

الملخص

بطاريات أيونات الليثيوم ذات الحالة الصلبة تعد المصدر الأمثل للطاقة وخاصة الأجهزة المتطورة صغيرة الحجم, و ذلك لانها امنة و ذات طاقة استيعابية عالية. على الرغم من مميزاتها إلا أنها مازالت تواجه من تغييرات كبيرة في أحجام المواد داخل أجزاء الكاثود. هذه التغيرات تؤدي إلى حصول تشوهات و أحمال عالية على المواد داخل الكاثود و بالتالي تؤدي إلى حدوث التشققات داخل المواد. واحدة من الحلول لهذه المشكلة هو اضافة اللدائن بكميات معينة الى مواد الكاثود بدون التأثير على فعاليتها لتوصيل الأيونات . لإيجاد أفضل نسبة من هذه المواد المضافة تم عمل نموذج لتصرفها داخل مواد الكاثود بوساطة دراسة حاسوبية. هذه الدراسة و باعتمادها على نظرية التشوهات الصغيرة أظهرت تحسنا للاداء و اظهرت نتائج الاحمال جيدة المجمل لكن ليست دقيقة لتمثيل تصرف اللدائن. لإيجاد نتائج التصرف مفرط الليونة للدائن يجب اتباع و توظيف نظرية التغير أو التشوهات الكبيرة. لذلك علينا اشتقاق المعادلات المطلوبة لتمثيل هذا التصرف فوق المرن و القابل للضغط باستخدام نظرية التشوهات الكبيرة. سوف نشغل المعادلات المشتقة باستخدام برنامج FORTRAN و نستخدم الناتج منه لدمج التصرف الجديد للدائن باستخدام برنامج ANSYS وكذلك برامج GeoDict. النتائج الاولية للأحمال لنموذج تصرف هذه المواد أظهرت قياسات و نتائج أدق لوصف التصرف فوق المرن. نتيجة لذلك هذا النموذج للتصرف فوق المرن يمكن الاعتماد عليه و تطويره في أعمال مستقبلية.